

Spring 2015

# Characterization of cell-type specific responses in *C. elegans* experiencing misfolded protein stress: How do some cells save themselves while others die?

Courtney A. Matson  
*James Madison University*

Erin N. Wallace  
*James Madison University*

Follow this and additional works at: <https://commons.lib.jmu.edu/honors201019>

 Part of the [Biology Commons](#), and the [Biotechnology Commons](#)

---

## Recommended Citation

Matson, Courtney A. and Wallace, Erin N., "Characterization of cell-type specific responses in *C. elegans* experiencing misfolded protein stress: How do some cells save themselves while others die?" (2015). *Senior Honors Projects, 2010-current*. 44.  
<https://commons.lib.jmu.edu/honors201019/44>

This Thesis is brought to you for free and open access by the Honors College at JMU Scholarly Commons. It has been accepted for inclusion in Senior Honors Projects, 2010-current by an authorized administrator of JMU Scholarly Commons. For more information, please contact [dc\\_admin@jmu.edu](mailto:dc_admin@jmu.edu).

Characterization of Cell-type Specific Responses in *C. elegans*  
Experiencing Misfolded Protein Stress: How Do Some Cells  
Save Themselves While Others Die?

---

An Honors Program Project Presented to  
the Faculty of the Undergraduate  
College of Science and Mathematics  
James Madison University

---

by Courtney Matson and Erin Wallace

---

---

Accepted by the faculty of the Department of Biology, James Madison University, in partial fulfillment of the requirements for the Honors Program.

FACULTY COMMITTEE:

HONORS PROGRAM APPROVAL:

---

Project Advisor: Timothy Bloss, Ph.D.,  
Associate Professor, Department of Biology

---

Philip Frana, Ph.D.,  
Interim Director, Honors Program

---

Reader: Kyle Seifert, Ph.D.,  
Associate Professor, Department of Biology

---

Reader: Kimberly Slekar, Ph.D.,  
Associate Professor, Department of Biology

---

---

PUBLIC PRESENTATION

This work is accepted for presentation, in part or in full, at Biosymposium on April 17<sup>th</sup> 2015.

**Characterization of Cell-type Specific Responses in *C. elegans*  
Experiencing Misfolded Protein Stress: How Do Some Cells  
Save Themselves While Others Die?**

**Courtney Matson and Erin Wallace**

**An Honors Thesis submitted to the Biology Department of**

**JAMES MADISON UNIVERSITY**

**April 2015**

## Contents

<b>Abstract</b>	6
<b>1 Introduction</b>	7
<b>2 Methods</b>	
2.1 Care and Maintenance of <i>C. elegans</i>	15
2.2 <i>hsp-4</i> ::GFP and Cell Lineage Reporter Strains	15
2.3 Bacterial Culture Maintenance	15
2.4 Mounting <i>C. elegans</i> for microscopy	16
2.5 RNA Interference Plates and Cultures	16
2.6 Male Generation	17
2.7 Worm Strain Generation Through Genetic Crosses	17
2.8 RNAi Assay for Embryo Characterization	18
2.9 RNAi Assay for Colocalization of Heat Shock Protein 4 and Gut Cell	19
2.10 Confocal Microscopy for Gut Characterization Embryos	20
2.11 Confocal Microscopy for Colocalization of Heat Shock Protein 4 and Gut Cell	21
2.12 Digital Analysis with ImageJ for Gut Characterization Embryos	22
2.13 Digital Analysis with ImageJ for Colocalization of Heat Shock Protein 4 and Gut Cell	22
2.14 Statistical Analysis for Gut Characterization Embryos	22

<b>3 Results</b>	
3.1 Depletion of the ICD-1 and/or ICD-2 subunit significantly affects percentage of embryos expressing RFP signal	24
3.2 Depletion of the ICD-1 and/or ICD-2 subunit significantly affects levels of RFP expression in embryos	27
3.3 Depletion of the ICD-1 and/or ICD-2 subunit significantly affects intensity of RFP signal in embryos	37
3.4 Colocalization of HSP-4::GFP/Gut::RFP under control treatment	46
<b>4 Discussion</b>	49
<b>5 Acknowledgments</b>	56
<b>6 References</b>	57

## List of figures

1 The Unfolded Protein Response (UPR) mechanism engaged in the presence of misfolded protein stress.	12
2a RNAi assay protocol diagram for Gut Characterization.	19
2b RNAi assay protocol diagram for Colocalization of Heat Shock Protein 4 and Gut Cell.	20
3 RFP signal in three-fold stage embryos after 24 hours of exposure to specific RNAi treatments.	27
4 RFP signal in four-fold stage embryos after 24 hours of exposure to specific RNAi treatments.	28
5 Average RFP expression levels for three-fold stage embryos exposed to specific RNAi treatments for increasing amounts of time.	32
6 Average RFP expression levels for four-fold stage embryos exposed to specific RNAi treatments for increasing amounts of time.	36
7 Average RFP intensity levels for three-fold stage embryos exposed to specific RNAi treatments for increasing amounts of time.	41
8 Average RFP intensity levels for four-fold stage embryos exposed to specific RNAi treatments for increasing amounts of time.	45
9 Adult HSP-4::GFP/Gut::RFP worm under control treatment.	48

## **ABSTRACT**

To maintain viability, cells must resolve misfolded protein stress; the inability to do so often triggers cell death, most notably in neurons during neurodegenerative disease. The NAC is a highly conserved translational chaperone essential for protein folding and localization to organelles throughout the cell. In *C. elegans*, depletion of the NAC initiates misfolded protein stress specifically in the endoplasmic reticulum, inducing a response that upregulates the HSP-4 chaperone in an attempt to prevent cell death. This upregulation is robust but not uniform, and deficient in regions containing neurons. We are characterizing this non-uniform stress response to determine if HSP-4 upregulation is cell-specific and correlates with survival. Additionally, there is evidence that the NAC may function in engaging premature and/or atypical differentiation under stress conditions. We've developed a protocol that characterizes the differentiation patterns and stress responses in NAC-depleted *C. elegans*. Our results indicate that NAC-depleted *C. elegans* have altered gut cell differentiation patterns when compared to control treatments. Furthermore, control studies were conducted to determine baseline patterns of HSP-4 expression in relation to the location of gut cells. Future studies will investigate differentiation patterns of muscle and neuronal cells in NAC-depleted *C. elegans* as well as characterizing the upregulation of HSP-4 in gut, muscle, and neuronal cells within NAC-depleted *C. elegans*.

## **INTRODUCTION**

Proteins are versatile macromolecules essential for the function of every cell in the body. The structure of a protein determines its function and is itself defined by the content and order of the amino acids that make up the protein. Amino acids form proteins through dehydration synthesis reactions in which a peptide bond is formed between two adjacent amino acids. The linking of amino acids forms a chain of peptide bonds that leads to the formation of the primary structure of a polypeptide. As the chain emerges from the ribosomal complex during translation, adjacent amino acids interact via hydrogen bonding to form twists and folds that result in secondary structures, e.g. alpha helical structures and beta-pleated sheets. Subsequently, secondary structures interact with each other depending on the nature of their specific amino acid R-groups, which form ionic bonds, disulfide bridges and hydrophobic interactions and generate the tertiary structure of the polypeptide. Many amino acid chains become immediately functional once they have folded into their proper structure, while some interact with other amino acid chains, forming quaternary structure required for functionality<sup>1</sup>

Proper protein folding during translation followed by maintenance of that folded structure are essential for protein function and therefore cell viability. The flow of information required to generate a functional protein initiates from the nucleus and terminates in the cytoplasm: a gene is transcribed into a primary mRNA that is processed to make a mature mRNA. These mRNAs are read by ribosomal complexes, generating a chain of amino acids that interact to create the initial structure of the polypeptide. The early stages of protein folding are the foundation for the final protein structure and if not properly conducted, will result in a misfolded protein that is either nonfunctional or

differentially functioned. Misfolded proteins often result from exogenous stress on the cell, and can accumulate in different cellular compartments. Misfolded proteins can cause damage by forming aggregates that interact with cellular organelles and/or perpetuating the misfolding of other proteins<sup>2</sup>. Specifically, the endoplasmic reticulum (ER) is susceptible to aggregation of misfolded protein during periods of stress generated by heat, toxins, aging, and nutrient deficiencies; stress events that generate misfolded protein in the ER can lead to the death of the cell if the stress is chronic or acute<sup>3</sup>

Under normal conditions, the ER is responsible for the first step in proper protein folding. The rough ER is responsible for synthesizing nascent polypeptides that will become functional proteins whereas the smooth ER is responsible for maintaining and processing these polypeptides<sup>4</sup>. Under stress conditions, the accumulation of misfolding peptide chains can overwhelm the folding mechanisms of the ER, resulting in accumulation and aggregation within the lumen<sup>4</sup>. To prevent this occurrence, the stressed cell engages the ER-specific unfolded protein response (UPR), which initiates cell-saving mechanisms to help alleviate the misfolded protein accumulation and aid the cell in coping with cell stress<sup>5</sup>. When the misfolded protein stress is too acute or chronic to allow for timely resolution, the UPR will initiate mechanisms that kill the cell, primarily via apoptosis; the UPR-mediated outcome is what putatively links ER misfolded protein stress to a number of human diseases. By way of an example, most, if not all, neurodegenerative disease pathologies include the accumulation of misfolded proteins<sup>6</sup>. There are multiple hypotheses regarding the origin of the protein accumulation in neurodegenerative diseases and its contribution to disease progression, including disrupted function of the ER due to high levels of misfolded proteins not processed

efficiently before aggregating<sup>2,4</sup>. Ultimately, the accumulation of misfolded proteins is thought to trigger cell death as a mechanism to protect the organism; this cell death is what likely links misfolded protein stress and the subsequent induction of the UPR to the apoptotic loss of neurons observed during neurodegeneration<sup>7</sup>.

To establish and maintain properly folded proteins and avoid the damage associated with misfolded protein stress, the cell expresses chaperones, a family of proteins dedicated solely to aiding in protein folding. Chaperones are expressed throughout the cell's life and constitute the proteostasis network that regulates both nascent protein folding and the refolding of misfolded proteins<sup>8</sup>. Chaperones work individually and in combination to control the folding environment of polypeptides; they prevent nascent chain misfolding during translation, and refold misfolded proteins to their native states during stress. When misfolded protein stress becomes acute and/or chronic, chaperones are also known to shuttle misfolded proteins to degradation pathways<sup>9,10</sup>. Individual chaperone functions have been characterized<sup>11</sup> as well as the inter-related interactions that constitute the chaperome, a complex network of cooperative chaperone relationships that regulate the structures of both nascent proteins and misfolded proteins<sup>8</sup>.

Within the chaperone family are heat shock proteins (HSPs), a class of chaperones originally associated with heat stress that bind polypeptides and assist with folding. Heat shock proteins are ubiquitous and abundant, comprising approximately 1-2 percent of the total proteins within a cell<sup>12</sup>. Their primary role is to prevent any misfolding events and aggregation during cell stress<sup>13</sup>. There are multiple classes of heat shock proteins, classified by the molecular weight of the founding member, all with specific functions: small HSPs, HSP40, HSP70, HSP90, and HSP100. Small HSPs

prevent the initial accumulation of aggregated proteins. If aggregates occur, HSP40 chaperones deliver the aggregated proteins to HSP70 chaperones, which associate with HSP100 chaperones to dissolve and reactivate misfolded proteins in an ATP-dependent manner. Once these aggregates have been properly refolded, HSP90 chaperones maintain this folded state<sup>12,14</sup>. Of these classes, HSP70 members have been extensively studied and highly conserved throughout evolution, with a subset, including BiP, specific to the management of misfolded protein in the ER<sup>13</sup>.

In addition to the HSPs, there are other classes of chaperones less well characterized, but still essential for proper protein folding, including those that bind to nascent polypeptides as they emerge from the ribosome, otherwise known as translational chaperones. The nascent polypeptide associated complex (NAC) is a translational chaperone complex that exists as a heterodimer with two subunits, alpha and beta; the beta subunit is responsible for the NAC's association with the ribosomal complex<sup>15</sup>. Specifically, the NAC is responsible for promoting nascent protein folding as well as protein localization during translation, and therefore directly maintains proteostasis and cell viability<sup>16,17</sup>. Therefore, the NAC plays an essential role in the control of protein folding and localization to different organelles and the complete loss of the NAC causes lethal phenotypes in many organisms, including mice and *Drosophila melanogaster*.

While the initial characterizations of the NAC were performed primarily in yeast, recently important insights into the functions of this complex have been gained in metazoans, including *Caenorhabditis elegans* (*C. elegans*). As with mice and *Drosophila*, a complete genetic knockout of either subunit of the NAC in *C. elegans* is embryonically lethal<sup>18</sup>. As such, knockdown experimental procedures of the NAC, e.g. through the use

of RNA interference, is necessary for investigating the roles of this complex in protein folding. Through depletion of one or the other subunit, it has been determined the depletion of the NAC in *C. elegans* results in accumulation of misfolded protein stress in the ER, presumably due to the mislocalization of poorly folded proteins to the ER in the absence of NAC's translational chaperone function<sup>16</sup>. This accumulation results in the induction of the UPR, which initiates both cell-saving and cell-killing responses depending on the severity and duration of the stress<sup>19</sup>.

The UPR has three key proteins that are variably engaged during a stress response: IRE-1, ATF6, and PERK/PEK-1. The initial actions of the UPR engage several cell-saving mechanisms, including an attenuation of translation, increased chaperone expression, increased protein degradation and turnover, and expansion of the luminal area of the ER<sup>5</sup>. When these cell saving responses are unable to resolve the stress in a timely fashion, the UPR engages cell killing mechanisms to remove the damaged cell from the organism. These cell deaths are primarily via apoptosis, although UPR-mediated autophagy has also been shown to contribute in certain contexts (Figure 1). While the UPR has been previously characterized in the context of stress response, there is gathering evidence that the UPR is also engaged to drive the differentiation of certain cell types<sup>5,20</sup>.

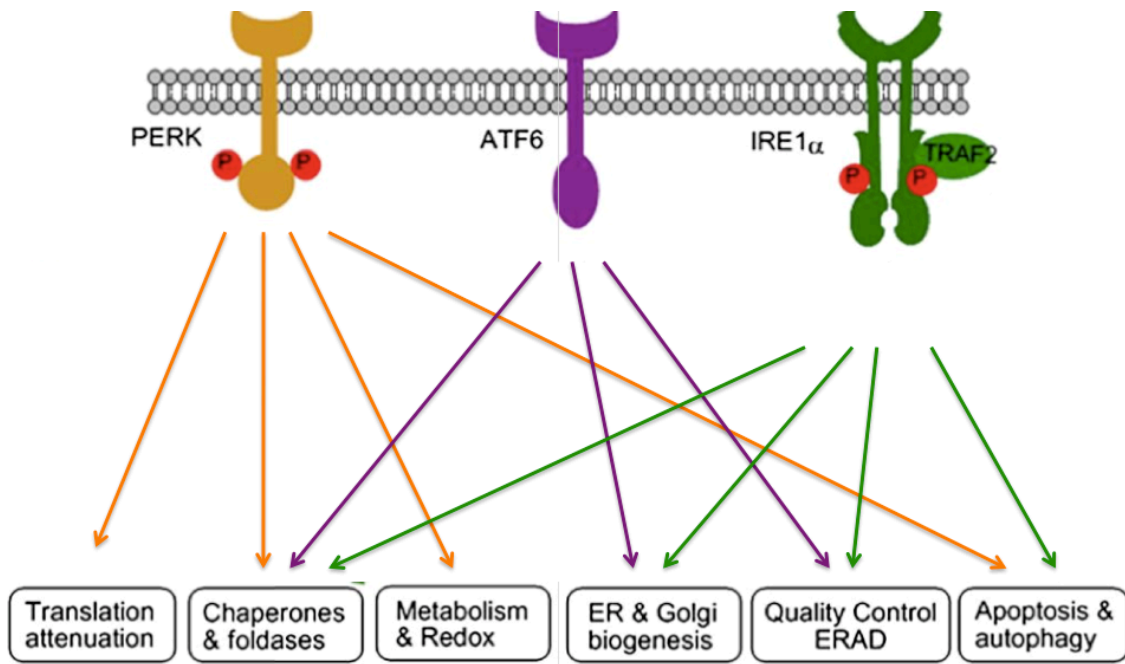


**Figure 1.** The Unfolded Protein Response (UPR) mechanism engaged in the presence of misfolded protein stress. The three key proteins of the UPR are IRE-1, ATF6, and PERK/PEK-1. The UPR engages several mechanisms, including translation attenuation, increased chaperone expression, increased protein degradation and turnover, and ER biogenesis during times of misfolded protein stress. The UPR engages cell killing mechanisms when the cell-saving mechanisms are unable to resolve the stress. These cell deaths are via apoptosis and autophagy. Figure adaptation<sup>21</sup>.

While the NAC is a heterodimer that functions as a translational chaperone, there is strong evidence that the subunits also function independently of each other. For alpha NAC, there is compelling evidence for a role as a transcription factor in the regulation of cell differentiation, consistent with alpha NACs ability to translocate from the cytoplasm to the nucleus when not bound by beta NAC<sup>22</sup>. Specifically, alpha NAC helps regulate osteoblast development in mice<sup>22,23</sup>. In this role, alpha NAC interacts with histone deacetylases to both upregulate and downregulate a suite of osteocalcin genes that promotes osteoblast maturation and bone mineralization during development<sup>24,25</sup>. In addition to its role in bone cell differentiation, alpha NAC acts as a positive regulator of erythroid cell differentiation although there are no specific mechanisms to elucidate this

pathway currently<sup>26</sup>. Initially identified and characterized in the context of its role in the NAC complex, alpha NAC itself appears to have a multitude of functions above and beyond the protein folding regulation and localization that it performs when bound to beta NAC.

Alpha NAC has been relatively well characterized in terms of its independent roles; less is known about the role(s) of beta NAC when not bound by alpha NAC. In the absence of alpha NAC, beta NAC has the ability to stop ribosome binding to the ER, likely a reflection of its role to control protein localization during translation. Beyond this analysis, characterization of beta NAC has been performed in the context of depletion of the subunit<sup>15</sup>. Initial studies of beta NAC in *C. elegans* identified it as a repressor of apoptosis. Specifically, a decrease in beta NAC levels increases apoptosis early in embryogenesis, with neurons being particularly susceptible<sup>18</sup>. Similarly, in human cell lines, the down-regulation of beta NAC has been correlated with apoptosis<sup>27,28</sup>. Recent evidence links beta NAC's ability to suppress apoptosis and prevention of misfolded protein stress to the activation of the UPR and subsequent induction of apoptosis<sup>16</sup>. The evidence of beta NAC as an inhibitor of apoptosis is based solely on phenotypes generated in its absence, making it impossible to determine if these results are due to the loss specifically of beta NAC, the loss of the NAC, or both. In support of beta NAC having an anti-apoptotic function above and beyond its role in the NAC, overexpression of beta NAC in the presence of normal expression levels of alpha NAC leads to the survival of cells that are normally eliminated by apoptosis during embryonic development<sup>29</sup>.

There is ample evidence that the NAC and its individual subunits play important roles in the management of misfolded protein stress in the ER, as well as potential roles in the control of certain cell differentiation programs. There is also evidence that stress induced by the depletion of the NAC is tolerated differentially by different cell types, with neurons being particularly susceptible to apoptotic cell death. Our research has focused on the link between the depletion of the NAC and cell-specific responses, including the putative role(s) of the individual subunit when in excess to its binding partner. To determine the role of the NAC in cell specific responses to misfolded protein stress, *C. elegans* embryos with fluorescently tagged cell lineages, specifically intestinal cells, were manipulated. In order to characterize both the stress response and the timing of cell differentiation in these embryos, alpha NAC, beta NAC or both were depleted. Our hypothesis was that the depletion of either NAC subunit will induce UPR cell-saving responses in gut cells, while a relative abundance of alpha NAC during the depletion of beta NAC will drive gut cells to differentiate earlier relative to gut cells in wild-type organisms.

## **METHODS**

### Care and Maintenance of *C. elegans*

*C. elegans* wild-type and mutant worms with GFP and/or RFP reporter constructs were maintained on Nematode Growth Medium (NGM) (Carolina Biological) plates that contained the *Escherichia coli* strain, OP50-1, as a food source. Worms were maintained at 22 °C. Short term maintenance involved the transfer of adults to freshly seeded OP50-1/ NGM plates every 3-4 days.

### *hsp-4*::GFP and Cell Lineage Reporter Strains

Heat Shock Protein 4::Green Fluorescent Protein (*hsp-4*::GFP), the *C. elegans* homolog of Heat Shock Protein 70, and Gut::Red Fluorescent Protein (Gut::RFP) strains were acquired from the *Caenorhabditis* Genetics Center (CGC) at the University of Minnesota. The HSP-4 construct consists of the gene expression control region of the specified *hsp-4* fused to GFP. The Gut::RFP strain contains a fluorescently tagged P<sub>vha6</sub>::mRFPPTS1 attached to the *unc119* gene, localizing RFP signal to peroxisomes in intestinal cells.

### Bacterial Culture Maintenance

Bacterial cultures of *E. coli* OP50-1 and strains with RNAi plasmids were prepared weekly using Luria Broth culture media. Cultures were prepared with 10mL of Luria Broth and a pure culture inoculate of the respective *E. coli* strain. Antibiotics were added to the cultures to prevent unwanted growth of other microorganisms; 50 ug /mL ampicillin for RNAi plasmid strains and 50 ug /mL streptomycin for OP50-1. Cultures were incubated with shaking at 37 °C for 12 hours. After 12 hours, cultures were transferred to sterile 15mL tubes and refrigerated at 3.6 °C.

### Mounting *C. elegans* for microscopy

Slides were prepared by placing a small amount, approximately 100uL, of liquefied bacteriological agar onto a slide and pressing an additional slide to allow the liquefied agar to spread. The slides were allowed to sit for approximately two minutes before removing the top slide to expose the thin layer of agar. Approximately 30uL of M9 salt solution (22mM  $\text{KH}_2\text{PO}_4$ , 11mM  $\text{Na}_2\text{HPO}_4 \cdot 7\text{H}_2\text{O}$ , 85mM  $\text{NaCl}$ , 1mM  $\text{MgSO}_4$ ) was placed onto the center of the thin agar layer to allow for embryo transfer. Approximately 30uL of 3mM levamisole solution, suspended in M9, was placed onto the center of the thin agar layer to allow for adult transfer. Organisms were transferred from plates, either NGM agar seeded with *E.coli* OP50-1 or RNAi plates seeded with *E.coli* containing respective plasmids for dsRNA, to slides. The excess bacteria on the slide were removed from the M9 salt solution using a toothpick with an attached eyelash to move the bacteria out of the solution. This was done to clear the agar layer of bacteria in order to maintain a clear visual field for microscopy. Once the bacteria were removed from the solution, a coverslip was added to the slide. The sides of the coverslip were sealed to prevent the slide from drying out during observation.

### RNA Interference Plates and Cultures

To reduce ICD-1 and ICD-2 protein levels, RNA interference (RNAi) assay was employed. RNAi assay utilizes double-stranded (ds) RNA specific to the mRNA of a targeted gene to reduce the levels of the corresponding protein. The gene products of *icd-1* and *icd-2* were targeted by RNAi assays to determine the effects of reductions of ICD-1 and ICD-2 proteins on the expression of gut cells and the HSP-4 protein. Feeder bacteria expressing the appropriate dsRNA were obtained from Addgene, and grown from single

colonies in liquid LB by shaking overnight at 37°C. The dsRNA specific to *icd-1* and *icd-2* genes were introduced into larval worms, specifically L4 larvae, using a feeding method in which NGM plates were seeded with a culture of *E. coli* OP50-1 constructed with a plasmid with dsRNA that targeted one or the other subunit. RNAi plates were made by combining 4.5g NaCl, 25.5g agar, 3.75g peptone, 1.5mL of 2mg/mL uracil, 0.22g CaCl<sub>2</sub> 0.75g of 10mg/ml cholesterol in 1463mL of dH<sub>2</sub>O. This mixture was autoclaved, allowed to cool, and 37.5mL of phosphate buffer (pH 6), 1.5mL of 1M MgSO<sub>4</sub>, 15uL of 0.1M IPTG (for induction of the dsRNA expression) and 1.5mL of 25mg/mL ampicillin (for selection of the dsRNA-expressing plasmid) were added.

### Male Generation

Male *C. elegans* are typically produced through a chromosomal nondisjunction event during meiosis to produce an XO organism. To encourage a nondisjunction event, heat shock was employed. L4 larvae and early adult worms were moved to an NGM plate and incubated in 30°C for 6 hours. After 6 hours, the plate was removed and returned to 22°C and organisms were allowed to recover. After organisms recovered, progeny were observed with a dissection microscope to screen for males. Their characteristic arrow shaped tail and overall smaller appearance in comparison to hermaphroditic worms physically identified male *C. elegans*.

### Worm Strain Generation Through Genetic Crosses

Male worms were developed in the gut cell lineage reporter strain through heat shock. These males were crossed with hermaphrodites from the *hsp-4::GFP* strain and the F1

hermaphroditic progeny were and isolated on separate plates. Resulting F2 progeny were singled onto individual plates and their progeny were characterized for Gut::RFP and *hsp-4*::GFP presence. F2 worms producing 100% progeny showing both Gut::RFP and *hsp-4*::GFP were considered to be homozygous for the fluorescent alleles of both genes.

#### RNAi Assay for Embryo Characterization

Twenty to thirty L4 larvae were moved to a seeded RNAi (*icd-1*(RNAi), *icd-2*(RNAi), or *icd-1/icd-2*(RNAi)) plate, designated plate 1. After 12 hours, the original L4 worms were moved to plate 2. After worms were moved, the embryos on plate 1 were moved to a slide and analyzed. After 24 hours, the original L4 worms were moved to plate 3. After worms were moved, the embryos on plate 2 were moved to a slide and analyzed with confocal microscopy. After 36 hours, the original L4 worms were moved to plate 4. After worms were moved, the embryos on plate 3 were moved to a slide and analyzed. After 48 hours, the original L4 worms were taken off plate 4 and sacrificed. After worms were sacrificed, the embryos on plate 4 were moved to a slide and analyzed. To conduct a control treatment in which no RNAi was implemented, embryos were moved directly from an *E. coli* OP50-1 seeded NGM plate. All observation and analysis was conducted using confocal microscopy (Figure 2a).

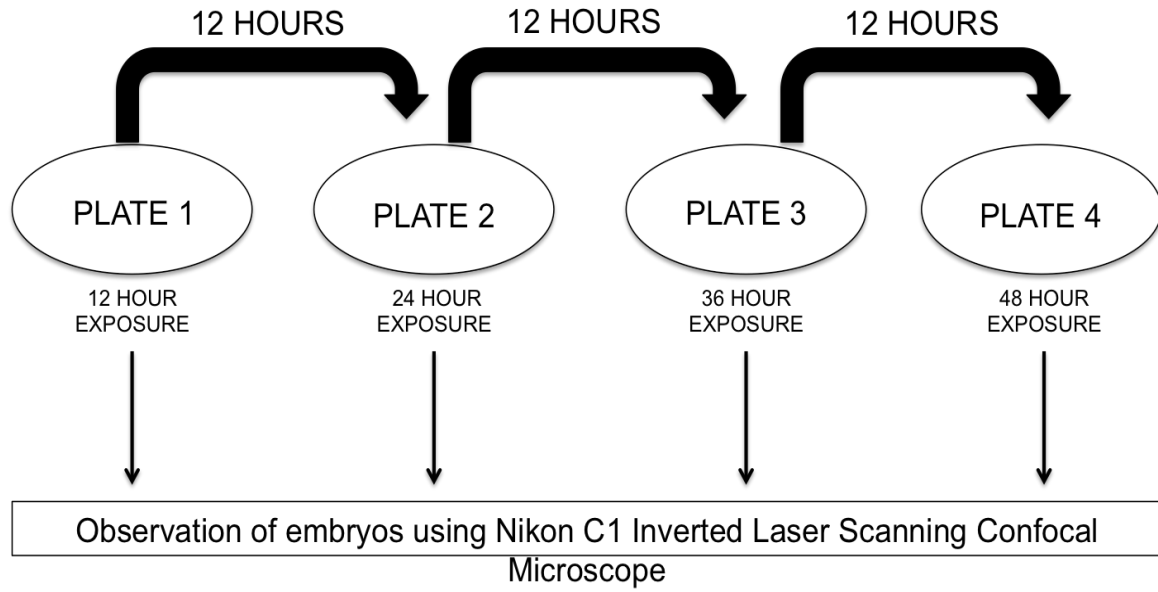


Figure 2a. RNAi assay protocol diagram for Gut Characterization.

#### RNAi Assay for Colocalization of Heat Shock Protein 4 and Gut Cell

Twenty to thirty L4 larvae were moved to a seeded RNAi (*icd-1*(RNAi), *icd-2*(RNAi), or *icd-1/icd-2*(RNAi)) plate, designated plate 1. After 12 hours, the original L4 worms were moved to plate 2. After worms were moved, the embryos on plate 1 were allowed to develop for 48 hours. The developed adults were moved to slide and analyzed. After 24 hours, the original L4 worms were moved to plate 3. After worms were moved, the embryos on plate 2 were allowed to develop for 48 hours. The developed adults were moved to slide and analyzed. After 36 hours, the original L4 worms were moved to plate 4. After worms were moved, the embryos on plate 3 were allowed to develop for 48 hours. The developed adults were moved to slide and analyzed. After 48 hours, the original L4 worms were taken off plate 4 and sacrificed. After worms were sacrificed, the embryos on plate 4 were allowed to develop for 48 hours. The developed adults were moved to slide and analyzed. To conduct a control treatment in which no RNAi was

implemented, adult worms were moved directly from an *E. coli* OP50-1 seeded NGM plate. All observation and analysis was conducted using confocal microscopy (Figure 2b).

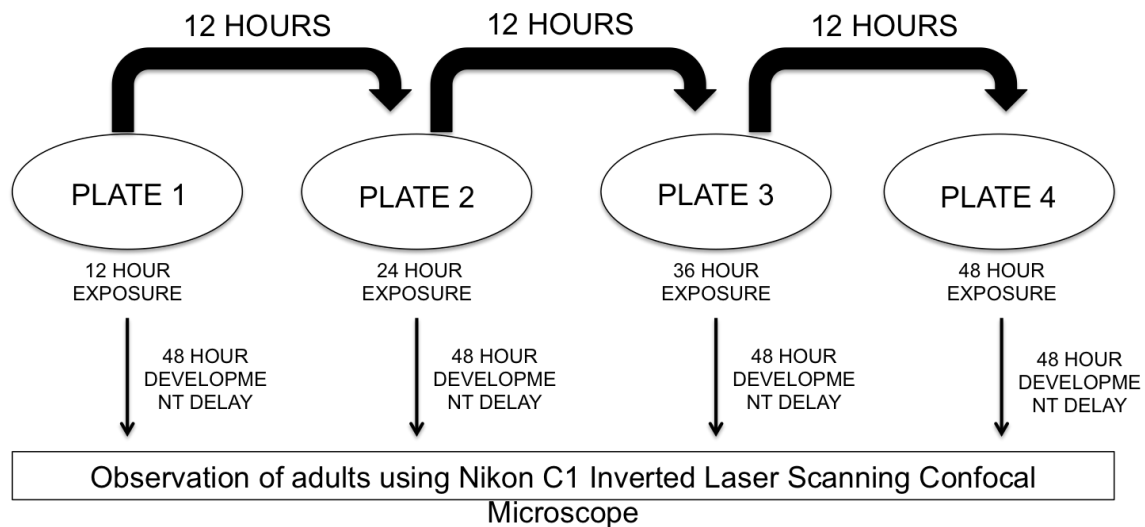


Figure 2b. RNAi assay protocol diagram for Colocalization of Heat Shock Protein 4 and Gut Cell.

### Confocal Microscopy for Gut Characterization Embryos

Prepared slides were observed using the Nikon C1 Inverted Laser Scanning Confocal Microscope. The fluorescent channels used were DsOrange (561nm) to detect Gut::RFP signal. For DsOrange, the fluorescent channels were set to the following thresholds: the HV/gain was set to 155, the offset was set to 0, and the laser power was set to 1.44. Each embryo was observed to determine stage and presence of signal. Stages were determined according to physical characteristics. The first identifiable stage is 390 to 420 minutes after first cleavage (comma stage) and is characterized by an invagination from the embryo shell. The second stage is 460 to 520 minutes after cleavage (two-fold stage) and is characterized by a larger invagination causing an elongation of the two sides of the

embryo forming a U-shaped organism. The third stage is 520 minutes to 620 minutes after cleavage (three-fold stage) and is characterized by an S-shaped organism that has three distinct folds within the embryo shell. The final stage before hatching is 620 minutes to 800 minutes after cleavage (four-fold stage) and is characterized by an elongated worm that is shaped like a four-fold. The number of embryos with or without signal was recorded for each stage. The total number of embryos (separated by stage) that displayed signal were recorded and divided by the total number of observed embryos. This value was recorded as a percentage of embryos with signal for each developmental stage. If there was signal present, a captured Differential Interference Contrast (DIC) image and fluorescent composite image was saved for further reference and analysis. Z stack fluorescent images were captured for each respective fluorescent channel for each embryo.

#### Confocal Microscopy for Colocalization of Heat Shock Protein 4 and Gut Cell

Prepared slides were observed using the Nikon C1 Inverted Laser Scanning Confocal Microscope. The fluorescent channels used were DsOrange (561nm) to detect Gut::*RFP* signal and GFP (488nm) to detect *hsp-4*::GFP signal. For DsOrange, the fluorescent channels were set to the following thresholds: the HV/gain was set to 155, the offset was set to 0, and the laser power was set to 1.44. For GFP, fluorescent channels were set to the following thresholds: the HV/gain was set to 133, the offset was set to 0, and the laser power was set to 1.44. A captured Differential Interference Contrast (DIC) image and fluorescent composite image was saved for further reference and analysis. Z stack

fluorescent images were captured for each respective fluorescent channel for each adult worm.

#### Digital Analysis with ImageJ for Gut Characterization Embryos

Confocal images were uploaded into ImageJ (National Institute of Health) utilizing the Bioformats plug-in to interpret the Nikon file format. Images were uploaded as a hyperstack in grayscale and subsequently analyzed. Utilizing the “Analyze Particle” function, the bounded region of the embryo, as identified from a captured DIC image, was analyzed to report the number of particles, the area of the region analyzed, and the mean intensity per stack in each hyperstack. These data were reported in a Microsoft Excel file and saved for further analysis.

#### Digital Analysis with ImageJ for Colocalization of Heat Shock Protein 4 and Gut Cell

Confocal files were uploaded into ImageJ (National Institute of Health) utilizing the Bioformats plug-in to interpret the Nikon files. Images were uploaded as a hyperstack in grayscale and subsequently analyzed. The channels of the DsOrange and GFP were split for colocalization analysis. The “Colocalization” plug-in was set to threshold values of 0. The composite image was then split into three channels: DsOrange, GFP, and Colocalized. The Colocalized channel was analyzed with the “Analyze Particle” function within the bounded region of the adult, as identified from a captured DIC image, to report the number of particles and the area of the region selected. These data were reported in a Microsoft Excel file and saved for further analysis.

#### Statistical Analysis for Gut Characterization Embryos

The excel files containing data from the ImageJ (National Institute of Health) analysis were compiled into a single Microsoft Excel file and analyzed. The average pixels per area unit were determined by dividing the sum of pixel counts by the sum of total area analyzed for each individual stack within the embryo to determine the overall average pixels per area unit for the entire hyperstack. Additionally, the mean pixel intensity per stack was averaged to determine the overall mean pixel intensity for the entire hyperstack. Data from comma and two-fold embryos was not analyzed due to lack signal in all observed embryos. Each data set from the three-fold and four-fold stages were separated based on time point (12 hour, 24 hour, 36 hour or 48 hour). Once data was compiled, the 48 hour time point was disregarded due to lack of discernable embryos and lack of data points for analysis. After data was compiled by time point and by stage, the data were averaged and standard deviation was determined for each time point and stage for each RNAi treatment. A two-way ANOVA was conducted to compare different time points of each RNAi treatment separated by stage for mean pixels per area unit and mean pixel intensity. Additionally, a Tukey post-hoc test was conducted to determine any statistically significant difference between the time points for each treatment and stage. Another two-way ANOVA was conducted to compare different RNAi treatments at each time point separated by stage for mean pixels per area unit and mean pixel intensity. Additionally another Tukey post-hoc test was conducted to determine any statistically significant difference between the RNAi treatments for each time point and stage.

## **RESULTS**

### Depletion of the ICD-1 and/or ICD-2 subunit significantly affects percentage of embryos expressing RFP signal

To characterize the effect of NAC individual subunit depletion on the presence of gut cells, ICD-1, ICD-2, and ICD-1/ICD-2 depleted embryos were examined for reporter signal. Signal from the Gut::Red Fluorescent Protein (RFP) strain worm, containing a fusion gene, localizes an RFP signal to peroxisomes in intestinal cells. Therefore the presence of RFP is indicative of gut cell differentiation. During observation, the presence of RFP was only seen beginning in the third stage (520 minutes to 620 minutes after cleavage, three-fold stage) and continuing into the fourth stage (620 minutes to 800 minutes after cleavage, four-fold stage). The number of embryos with or without signal was recorded for each stage. The total number of embryos (separated by stage) that displayed RFP was recorded and divided by the total number of observed embryos. The number of embryos produced at the 48 hour time point was dramatically diminished, and those that were present were extremely disrupted morphologically as to be indiscernible due to the prolonged RNAi exposure. Therefore, the 48 hour time point was excluded from further data analysis.

The percentages of three-fold embryos with RFP signal during *icd-1*(RNAi) treatment by time points (12 hours, 24 hours, and 36 hours) were: 47.83%, 54.69%, and 38.00%, respectively, while during *icd-2*(RNAi) treatment, they were: 32.61%, 25.97%, and 16.16%, respectively. The percentages of three-fold embryos with RFP signal during *icd-1/icd-2*(RNAi) treatment by time points (12 hours, 24 hours, and 36 hours) were:

55.56%, 20.51%, and 29.73%, respectively. The percentage of untreated three-fold embryos with RFP signal was 90.91% (Table 1).

**Table 1.** Percentage of three-fold stage embryos with RFP signal in comparison to total number of embryos viewed during indicated RNAi treatment .

<b>Percentage of three-fold embryos with RFP signal</b>				
	<i>icd-1</i> (RNAi)	<i>icd-2</i> (RNAi)	<i>icd-1/icd-2</i> (RNAi)	<b>Control</b>
<b>12 hours</b>	47.83	32.61	55.56	90.91
<b>24 hours</b>	54.69	25.97	20.51	
<b>36 hours</b>	38.00	16.16	29.73	

The percentages of four-fold embryos with RFP signal during *icd-1*(RNAi) treatment by time points (12 hours, 24 hours, and 36 hours) were: 60.00%, 38.89%, and 52.94%, respectively while during *icd-2*(RNAi) treatment, they were: 44.44%, 66.67%, and 23.68%, respectively. The percentages of four-fold embryos with RFP signal during *icd-1/icd-2*(RNAi) treatment by time points (12 hours, 24 hours, and 36 hours) were: 66.67%, 53.33%, and 31.82%, respectively. The percentage of untreated four-fold embryos with RFP signal was 80.00% (Table 2).

**Table 2.** Percentage of four-fold stage embryos with RFP signal in comparison to total number of embryos viewed during indicated RNAi treatment.

<b>Percentage of four-fold embryos with RFP signal</b>				
	<i>icd-1</i> (RNAi)	<i>icd-2</i> (RNAi)	<i>icd-1/icd-2</i> (RNAi)	<b>Control</b>
<b>12 hours</b>	60.00	44.44	66.67	80.00
<b>24 hours</b>	38.89	66.67	53.33	
<b>36 hours</b>	52.94	23.68	31.82	

In general, as time of exposure to RNAi treatment increased, the percent of embryos with signal decreased. When three-fold embryos expressing RFP were compared, different localization patterns were present. Most strikingly, *icd-1*(RNAi) three-fold embryos displayed larger, punctate Gut::RFP aggregations relative to the other

treatment groups and the control treatment (Figure 3). Four-fold stage embryos expressing RFP during all RNAi treatments displayed large, punctate signals similar to *icd-1*(RNAi) three-fold embryos, but in all cases, this pattern was more widespread throughout the gut (Figure 4). To characterize and quantify the similarities and differences of Gut::RFP signal among the different treatment groups, all further data analyses were done on three-fold and four-fold embryos displaying fluorescent signal.

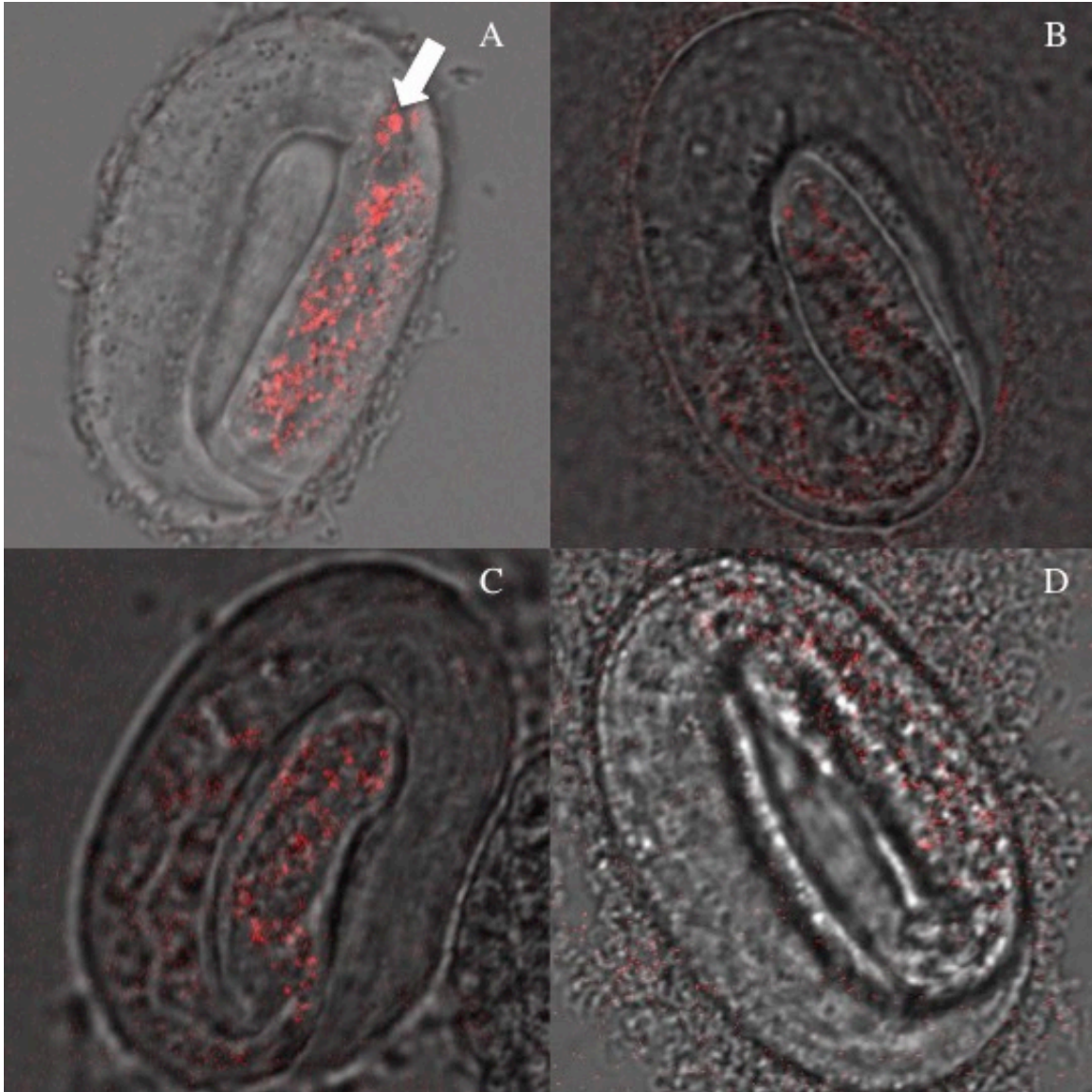


**Figure 3. RFP signal in three-fold stage embryos after 24 hours of exposure to specific RNAi treatments.** *C. elegans* with a Gut::RFP expression vector were fed (A) *icd-1*(RNAi)-specific bacteria, (B) *icd-2*(RNAi)-specific bacteria, (C) *icd-1*(RNAi)-specific bacteria and *icd-2*(RNAi)-specific bacteria, or (D) OP50-1 (*E. coli*) bacteria expressing no double stranded RNA for 24 hours, and their progeny embryos were randomly assessed for expression of RFP using confocal microscopy. DIC and fluorescent images were overlaid with ImageJ software. Arrow indicates large, punctate Gut::RFP signal.

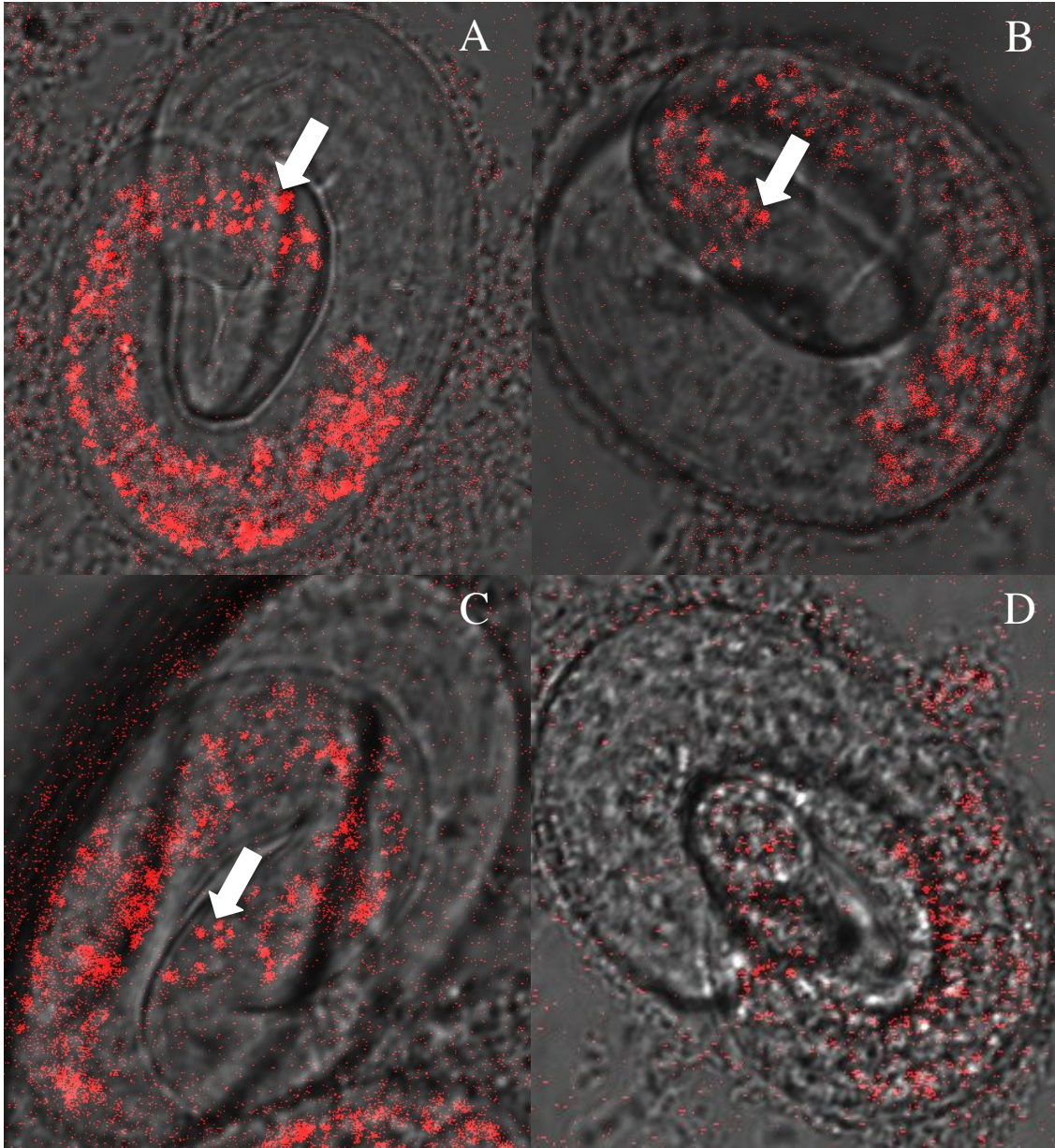


**Figure 4. RFP signal in four-fold stage embryos after 24 hours of exposure to specific RNAi treatments.** *C. elegans* with a Gut::RFP expression vector were fed (A) *icd-1*(RNAi)-specific bacteria, (B) *icd-2*(RNAi)-specific bacteria, (C) *icd-1*(RNAi)-specific bacteria and *icd-2*(RNAi)-specific bacteria, or (D) OP50-1 (*E. coli*) bacteria expressing no double stranded RNA for 24 hours, and their progeny embryos were randomly assessed for expression of RFP using confocal microscopy. DIC and fluorescent images were overlaid with ImageJ software. Arrow indicates large, punctate Gut::RFP signal.

Depletion of the ICD-1 and/or ICD-2 subunit significantly affects levels of RFP expression in embryos

The qualitative differences in RFP expression patterns observed between RNAi treatment groups led us to ask if depletion of different NAC subunits resulted in significant quantitative differences in RFP expression. One measure of these putative differences in expression is to quantify the amount of RFP fluorescence expressed in individual embryos, otherwise known as mean pixels (RFP signal) per area unit (the embryo).

To determine the effect of NAC individual subunit depletion on the amount of RFP expressed per embryo, ICD-1, ICD-2, and ICD-1/ICD-2 depleted embryos were examined and the mean pixels per area unit (arbitrary units) of each embryo was calculated from the image analysis data output. The mean pixels per area unit values for individual *icd-1*(RNAi) treated three-fold embryos by time points (12 hours, 24 hours, and 36 hours) were:  $78.26 \pm 22.55$ ,  $58.11 \pm 23.17$ , and  $58.10 \pm 21.04$ , respectively, while for *icd-2*(RNAi) treated embryos, mean pixels per area unit for the same time points were:  $61.45 \pm 19.57$ ,  $44.41 \pm 34.15$ , and  $51.38 \pm 42.73$ , respectively. The mean pixels per area unit for individual *icd-1/icd-2*(RNAi) treated three-fold embryos by time points (12 hours, 24 hours, and 36 hours) were:  $36.41 \pm 22.04$ ,  $46.29 \pm 14.41$ , and  $49.89 \pm 14.55$ , respectively. Untreated embryos displayed a mean pixels per area unit value of  $13.18 \pm 7.91$  (Table 3).

**Table 3.** Average level of RFP expression in three-fold embryos after exposure to specific RNAi treatments over time. Mean pixels per area unit (arbitrary units) for individual three-fold stage embryos exposed to *icd-1*(RNAi), *icd-2*(RNAi), or *icd-1/icd-2*(RNAi) were determined every 12 hours for 36 hours as a measure of RFP expression, and expressed as an average.

Average level of RFP expression in individual embryos				
	<i>icd-1</i> RNAi	<i>icd-2</i> RNAi	<i>icd-1/icd-2</i> RNAi	Control
<b>12 hours</b>	78.26 ± 22.55	61.45 ± 19.57	36.41 ± 22.04	13.18 ± 7.91
<b>24 hours</b>	58.11 ± 23.17	44.41 ± 34.15	46.29 ± 14.41	
<b>36 hours</b>	58.10 ± 21.04	51.38 ± 42.73	49.89 ± 14.55	

The results of these experiments were analyzed with a two-way ANOVA to determine the statistical significance between the treatments for each time point (Figure 5A-C). When the 12 hour time point of the three-fold stage embryos was compared, *icd-1*(RNAi), *icd-2*(RNAi), *icd-1/icd-2*(RNAi) and control treatments had statistically significant differences relative to each other with a p-value of <0.0001. A Tukey post-hoc test is conducted if there is a statistically significant difference present from the ANOVA. An ANOVA test examines if there are any differences present between the treatments where as a Tukey post-hoc test examines the differences between each treatment in comparison to the other individual treatments. A Tukey post-hoc test indicated that the differences lie between the RNAi (*icd-1*(RNAi), *icd-2*(RNAi), or *icd-1/icd-2*(RNAi)) and control treatments with an alpha value of 0.05. Additionally, the post-hoc test indicated statistically significant differences between all RNAi (*icd-1* to *icd-2*, *icd-1* to *icd-1/icd-2*, and *icd-2* to *icd-1/icd-2*) treatments with an alpha value of 0.05. When the 24 hour time point of the three-fold stage embryos was compared, RNAi (*icd-1*(RNAi), *icd-2*(RNAi), *icd-1/icd-2*(RNAi)) and control treatments had statistically significant differences with a p-value of <0.0001. A Tukey post-hoc test indicated that the differences lie between the RNAi (*icd-1*(RNAi), *icd-2*(RNAi), or *icd-1/icd-2*(RNAi)) and control treatments with an

alpha value of 0.05. When the 36 hour time point of the three-fold stage embryos was compared, RNAi (*icd-1*(RNAi), *icd-2*(RNAi), or *icd-1/icd-2*(RNAi)) and control treatments had statistically significant differences with a p-value of <0.0001. A Tukey post-hoc test indicated that the differences lie between the RNAi (*icd-1*(RNAi), *icd-2*(RNAi), *icd-1/icd-2*(RNAi)) and control treatments with an alpha value of 0.05.

The mean pixels per area unit data were also analyzed with a two-way ANOVA to determine the statistical significance between the time points within each treatment (Figure 5D-F). When the three-fold stage embryos exposed to *icd-1*(RNAi) treatment were compared, the 12 hour, 24 hour, and 36 hour had statistically significant differences with a p-value of 0.0030. A Tukey post-hoc test indicated that the differences lie between the 12 hour to the 24 hour and the 12 hour to the 36 hour with an alpha value of 0.05. When the three-fold stage embryos exposed to *icd-2*(RNAi) treatment were compared, the 12 hour, 24 hour, and 36 hour did not have a statistically significant difference with a p-value of 0.3452. When the three-fold stage embryos exposed to *icd-1/icd-2*(RNAi) treatment were compared, the 12 hour, 24 hour, and 36 hour did not have a statistically significant difference with a p-value of 0.2151.

At all time points (12, 24, and 36 hours) of exposure to RNAi treatments, the three-fold stage embryos exposed to the *icd-1*(RNAi) treatment had the largest value of mean pixels per area unit while the control treatment had the smallest value (Figure 5A-C). Under *icd-1*(RNAi) and *icd-2*(RNAi) treatments, the three-fold stage embryos within the 12 hour time point had the largest value of mean pixels per area unit whereas the 24 hour time point had the smallest value (Figure 5D-E). Alternatively, under *icd-1/icd-2*(RNAi) treatment, three-fold stage embryos within the 36 hour time point had the

largest value of mean pixels per area unit and the 12 hour time point had the smallest value (Figure 5F).

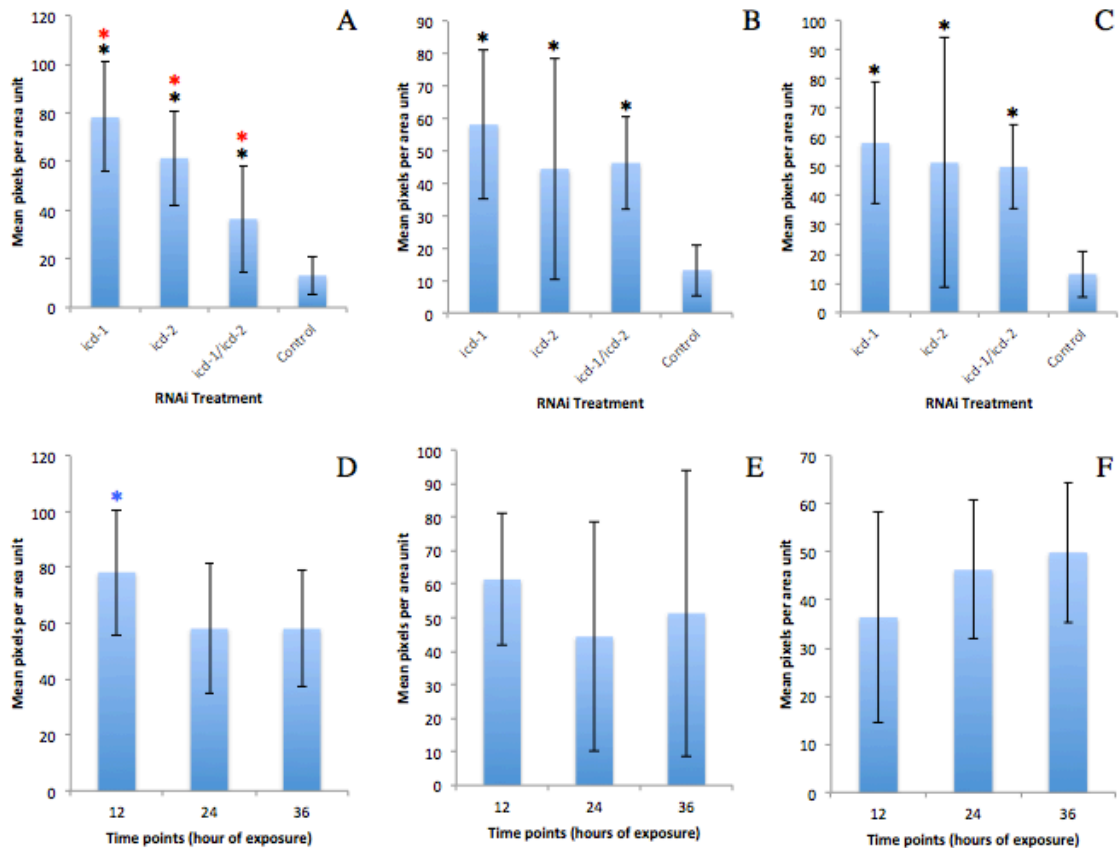


**Figure 5. Average RFP expression levels for three-fold stage embryos exposed to specific RNAi treatments for increasing amounts of time.** *C. elegans* with a Gut::RFP expression vector were exposed to the indicated RNAi treatment or OP50-1 (*E. coli*) bacteria expressing no double stranded RNA and their progeny embryos were randomly assessed for expression of RFP using confocal microscopy. Images were processed to determine the mean pixels per area unit with ImageJ software. (A) 12 hour time point of RNAi (*icd-1*(RNAi), *icd-2*(RNAi), or *icd-1/icd-2*(RNAi)) and control treatments. (B) 24 hour time point of RNAi (*icd-1*(RNAi), *icd-2*(RNAi), or *icd-1/icd-2*(RNAi)) and control treatments. (C) 36 hour time point of RNAi (*icd-1*(RNAi), *icd-2*(RNAi), or *icd-1/icd-2*(RNAi)) and control treatments. (D) 12, 24, and 36 hour time points for *icd-1*(RNAi) treatment. (E) 12, 24, and 36 hour time points for *icd-2*(RNAi) treatment. (F) 12, 24, and 36 hour time points for *icd-1/icd-2*(RNAi) treatment. Black asterisks indicate statistically significant difference between RNAi treatment and control treatment. Red asterisks indicate statistically significant difference between RNAi treatments. Blue asterisks indicate statistically significant difference between time points.

The mean pixels per area unit values for individual four-fold embryos exposed to *icd-1*(RNAi) treatment by time points (12 hours, 24 hours, and 36 hours) four-fold were:  $76.51 \pm 46.48$ ,  $43.84 \pm 18.01$ , and  $71.07 \pm 42.08$ , respectively, while for those exposed to *icd-2*(RNAi) treatment by time points (12 hours, 24 hours, and 36 hours) four-fold were:  $63.92 \pm 22.50$ ,  $37.31 \pm 22.41$ , and  $71.88 \pm 48.77$ , respectively. The mean pixels per area unit values for individual four-fold embryos exposed to *icd-1/icd-2*(RNAi) treatment by time points (12 hours, 24 hours, and 36 hours) four-fold were:  $39.25 \pm 31.10$ ,  $42.62 \pm 14.78$ , and  $45.23 \pm 20.38$ , respectively. Untreated embryos displayed a mean pixels per area unit value of four-fold  $15.58 \pm 6.07$  (Table 4).

**Table 4.** Average level of RFP expression in four-fold embryos after exposure to specific RNAi treatments over time. Mean pixels per area unit (arbitrary units) for individual four-fold stage embryos exposed to *icd-1*(RNAi), *icd-2*(RNAi), or *icd-1/icd-2*(RNAi) were determined every 12 hours for 36 hours as a measure of RFP expression, and expressed as an average.

<b>Average level of RFP expression in individual embryos Four-fold</b>				
	<i>icd-1</i> (RNAi)	<i>icd-2</i> (RNAi)	<i>icd-1/icd-2</i> (RNAi)	<b>Control</b>
<b>12 hours</b>	$76.51 \pm 46.48$	$63.92 \pm 22.50$	$39.25 \pm 31.10$	$15.58 \pm 6.07$
<b>24 hours</b>	$43.84 \pm 18.01$	$37.31 \pm 22.41$	$42.62 \pm 14.78$	
<b>36 hours</b>	$71.07 \pm 42.08$	$71.88 \pm 48.77$	$45.23 \pm 20.38$	

The mean pixels per area unit data were analyzed with a two-way ANOVA to determine the statistical significance between the treatments for each time point (Figure 6A-C). When the 12 hour time point of the four-fold stage embryos was compared, RNAi (*icd-1*(RNAi), *icd-2*(RNAi), *icd-1/icd-2*(RNAi)) and control treatments had statistically significant differences with a p-value of  $<0.0001$ . A Tukey post-hoc test indicated that the differences lie between the *icd-1*(RNAi) and *icd-2*(RNAi) treatments and the control with an alpha value of 0.05. Additionally, the post-hoc test indicated statistically

significant differences between *icd-1* RNAi and *icd-1/icd-2*(RNAi) treatments with an alpha value of 0.05. When the 24 hour time point of the four-fold stage embryos was compared, RNAi (*icd-1*(RNAi), *icd-2*(RNAi), *icd-1/icd-2*(RNAi)) and control treatments had statistically significant differences with a p-value of <0.0001. A Tukey post-hoc test indicated that the differences lie between the RNAi (*icd-1*(RNAi), *icd-2*(RNAi), or *icd-1/icd-2*(RNAi)) and the control treatment with an alpha value of 0.05. When the 36 hour time point of the four-fold stage embryos was compared, RNAi (*icd-1*(RNAi), *icd-2*(RNAi), or *icd-1/icd-2*(RNAi)) and control treatments had statistically significant differences with a p-value of <0.0001. A Tukey post-hoc test indicated that the differences lie between the *icd-1*(RNAi) and *icd-2*(RNAi) treatments and the control with an alpha value of 0.05.

The mean pixels per area unit data were also analyzed with a two-way ANOVA to determine the statistical significance between the time points within each treatment (Figure 6D-F). When the four-fold stage embryos exposed to *icd-1*(RNAi) treatment were compared, the 12 hour, 24 hour, and 36 hour did not have a statistically significant difference with a p-value of 0.0696. When the four-fold stage embryos exposed to *icd-2*(RNAi) treatment were compared, the 12 hour, 24 hour, and 36 hour had statistically significant differences with a p-value of 0.0205. A Tukey post-hoc test indicated that the differences lie between the 24 hour and 36 hour time points with an alpha value of 0.05. When the four-fold stage embryos exposed to *icd-1/icd-2*(RNAi) treatment were compared, the 12 hour, 24 hour, and 36 hour did not have a statistically significant difference with a p-value of 0.8831.

At the 12 and 24 hour time points of exposure to RNAi treatments, the four-fold stage embryos exposed to *icd-1*(RNAi) treatment had the largest value of mean pixels per area unit while the control treatment had the smallest value (Figure 6A-B). At the 36 hour time point of exposure to RNAi treatments, four-fold stage embryos exposed to the *icd-2*(RNAi) treatment had the largest value of mean pixels per area unit and the control treatment had the smallest value (Figure 6C). Under *icd-1*(RNAi) treatment, the four-fold stage embryos within the 24 hour time point had the largest value (Figure 6D). Additionally, under the *icd-2*(RNAi) treatment, four-fold stage embryos within the 12 hour time point had the largest value (Figure 6E). Finally, under *icd-1/icd-2*(RNAi) treatment, four-fold stage embryos within the 36 hour time point had the largest value of mean pixels per area unit and the 12 hour time point had the smallest (Figure 6F).

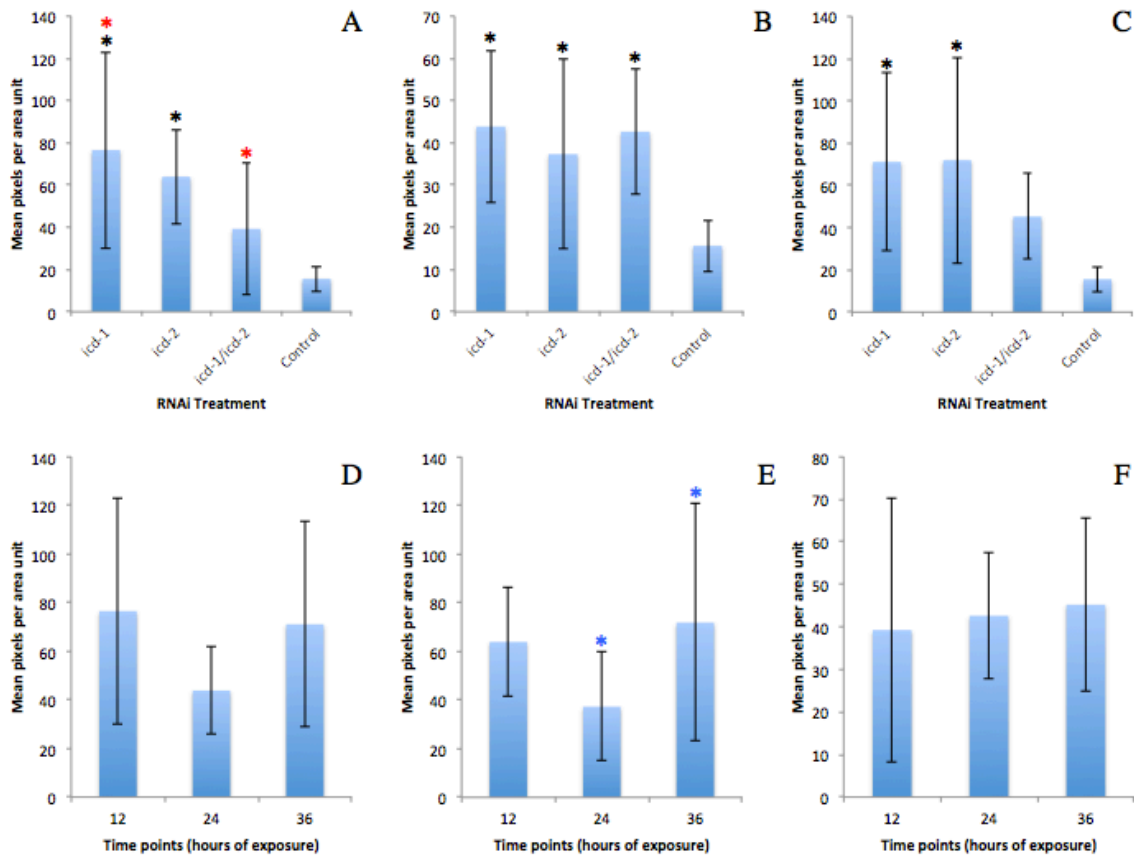


**Figure 6. Average RFP expression levels for four-fold stage embryos exposed to specific RNAi treatments for increasing amounts of time.** *C. elegans* with a Gut::RFP expression vector were exposed to the indicated RNAi treatment or OP50-1 (*E. coli*) bacteria expressing no double stranded RNA and their progeny embryos were randomly assessed for expression of RFP using confocal microscopy. Images were processed to determine the mean pixels per area unit with ImageJ software. (A) 12 hour time point of RNAi (*icd-1*(RNAi), *icd-2*(RNAi), or *icd-1/icd-2*(RNAi)) and control treatments. (B) 24 hour time point of RNAi (*icd-1*(RNAi), *icd-2*(RNAi), or *icd-1/icd-2*(RNAi)) and control treatments. (C) 36 hour time point of RNAi (*icd-1*(RNAi), *icd-2*(RNAi), or *icd-1/icd-2*(RNAi)) and control treatments. (D) 12, 24, and 36 hour time points for *icd-1*(RNAi) treatment. (E) 12, 24, and 36 hour time points for *icd-2*(RNAi) treatment. (F) 12, 24, and 36 hour time points for *icd-1/icd-2*(RNAi) treatment. Black asterisks indicate statistically significant difference between RNAi treatment and control treatment. Red asterisks indicate statistically significant difference between RNAi treatments. Blue asterisks indicate statistically significant difference between time points.

The mean pixels per area unit data were also analyzed with a Student's T-test to determine the statistical significance between the stages for each time point within each treatment (Table 5). The comparison of the 24 hour time point within the *icd-1*(RNAi)

treatment between the three-fold and the four-fold stage embryos had a statistically significant difference with a p-value of 0.0446. The remainder of the comparisons of each individual time point for each specific RNAi treatment between the two stages of embryos did not show any statistically significant differences as indicated by p-values greater than 0.05 (Table 5).

**Table 5.** Calculated p-values from Student’s T-tests for the comparison of the mean pixels per unit area of three-fold and four-fold stage embryos relative to each other.

	<i>icd-1</i> (RNAi)			<i>icd-2</i> (RNAi)			<i>icd-1/icd-2</i> (RNAi)		
	12 hours	24 hours	36 hours	12 hours	24 hours	36 hours	12 hours	24 hours	36 hours
<b>p-value</b>	0.887	0.044	0.282	0.581	0.458	0.284	0.823	0.623	0.577

Overall from the Student’s T test, the three-fold and four-fold stages were not significantly different for expression of RFP at any time point for any of the RNAi treatments. However, the *icd-1*(RNAi) at the 24 hour time point was statistically significant between three-fold and four-fold stage embryos. Conversely, both three-fold and four-fold stage embryos showed significant differences in RFP expression at all time points for all RNAi treatments (*icd-1*(RNAi), *icd-2*(RNAi), or *icd-1/icd-2*(RNAi)) when compared to controls.

Depletion of the ICD-1 and/or ICD-2 subunit significantly affects intensity of RFP signal in embryos

The qualitative differences in the intensity of RFP signal, particularly in the large punctate structures observed between RNAi treatment groups (Figures 3 and 4) led us to ask if depletion of different NAC subunits resulted in significant quantitative differences in intensity of RFP signal. Such differences may correlate strength of stress response

and/or rate of progression through differentiation with specific RNAi treatments. One measure of these putative differences in signal intensity is to quantify the strength of RFP fluorescence expressed in each individual embryo in a given treatment group, otherwise known as mean pixel intensity.

To determine the effect of NAC individual subunit depletion on the intensity of RFP signal in individual embryos, ICD-1, ICD-2, and ICD-1/ICD- 2 depleted embryos were examined and the mean pixel intensity (arbitrary units) was calculated from the image analysis output. The mean intensity values for three-fold embryos exposed to *icd-1*(RNAi) treatment by time points (12 hours, 24 hours, and 36 hours) were:  $627.97 \pm 224.31$ ,  $588.91 \pm 119.09$ , and  $554.69 \pm 65.96$ , respectively, while those exposed to *icd-2*(RNAi) treatment by time points (12 hours, 24 hours, and 36 hours) were:  $443.73 \pm 44.17$ ,  $418.70 \pm 42.69$ , and  $425.31 \pm 23.63$ , respectively. The mean intensity values for three-fold embryos exposed to *icd-1/icd-2*(RNAi) treatment by time points (12 hours, 24 hours, and 36 hours) were:  $631.92 \pm 48.09$ ,  $582.04 \pm 27.63$ , and  $583.62 \pm 64.27$ , respectively. The mean intensity value for the control treatment was  $1511.71 \pm 330.52$  (Table 6).

**Table 6.** Average intensity of RFP signal in three-fold embryos after exposure to specific RNAi treatments over time. Mean pixel intensity (arbitrary units) for three-fold stage embryos exposed to *icd-1*(RNAi), *icd-2*(RNAi), or *icd-1/icd-2*(RNAi) were determined every 12 hours for 36 hours as a measure of RFP signal intensity and expressed as an average.

<b>Three Fold Mean Intensity</b>				
	<i>icd-1</i> (RNAi)	<i>icd-2</i> (RNAi)	<i>icd-1/icd-2</i> (RNAi)	<b>Control</b>
<b>12 hours</b>	$627.97 \pm 224.31$	$443.73 \pm 44.17$	$631.92 \pm 48.09$	$1511.71 \pm 330$
<b>24 hours</b>	$588.91 \pm 119.09$	$418.70 \pm 42.69$	$582.04 \pm 27.63$	
<b>36 hours</b>	$554.69 \pm 65.96$	$425.31 \pm 23.63$	$583.62 \pm 64.27$	

The mean pixel intensity data were analyzed with a two-way ANOVA to determine the statistical significance between the treatments for each time point (Figure 7A-C). When the 12 hour time point of the three-fold stage embryos was compared, RNAi (*icd-1*(RNAi), *icd-2*(RNAi), or *icd-1/icd-2*(RNAi)) and control treatments had statistically significant differences with a p-value of <0.0001. A Tukey post-hoc test indicated that the differences lie between the RNAi (*icd-1*(RNAi), *icd-2*(RNAi), or *icd-1/icd-2*(RNAi)) treatments and the control treatment with an alpha value of 0.05. When the 24 hour time point of the three-fold stage embryos was compared, RNAi (*icd-1*(RNAi), *icd-2*(RNAi), or *icd-1/icd-2*(RNAi)) and control treatments had statistically significant differences with a p-value of <0.0001. A Tukey post-hoc test indicated that the differences lie between the RNAi (*icd-1*(RNAi), *icd-2*(RNAi), or *icd-1/icd-2*(RNAi)) treatments and the control treatment with an alpha value of 0.05. When the 36 hour time point of the three-fold stage embryos was compared RNAi (*icd-1*(RNAi), *icd-2*(RNAi), or *icd-1/icd-2*(RNAi)) and control treatments had statistically significant differences with a p-value of <0.0001. A Tukey post-hoc test indicated that the differences lie between the RNAi (*icd-1*(RNAi), *icd-2*(RNAi), or *icd-1/icd-2*(RNAi)) treatments and the control treatment with an alpha value of 0.05.

The mean pixel intensity data were also analyzed with a two-way ANOVA to determine the statistical significance between the time points within each treatment. When the three-fold embryos exposed to *icd-1*(RNAi) treatment were compared, the 12 hour, 24 hour, and 36 hour did not have a statistically significant difference with a p-value of 0.2935. When the three-fold stage embryos exposed to *icd-2*(RNAi) treatment were compared, the 12 hour, 24 hour, and 36 hour did not have a statistically significant

difference with a p-value of 0.1613. When the three-fold stage embryos exposed to *icd-1/icd-2*(RNAi) treatment were compared, the 12 hour, 24 hour, and 36 hour did not have a statistically significant difference with a p-value of 0.0657.

At the 12 hour, 24 hour, and 36 hour time point of exposure to RNAi treatments, the three-fold stage embryos exposed to *icd-2*(RNAi) treatment had the smallest value of mean pixel intensity while the control treatment had the largest value (Figure 7A-C). Under RNAi (*icd-1*(RNAi), *icd-2*(RNAi), or *icd-1/icd-2*(RNAi)) treatment, the three-fold stage embryos within the 12 hour time point had the largest value (Figure 7D-F).

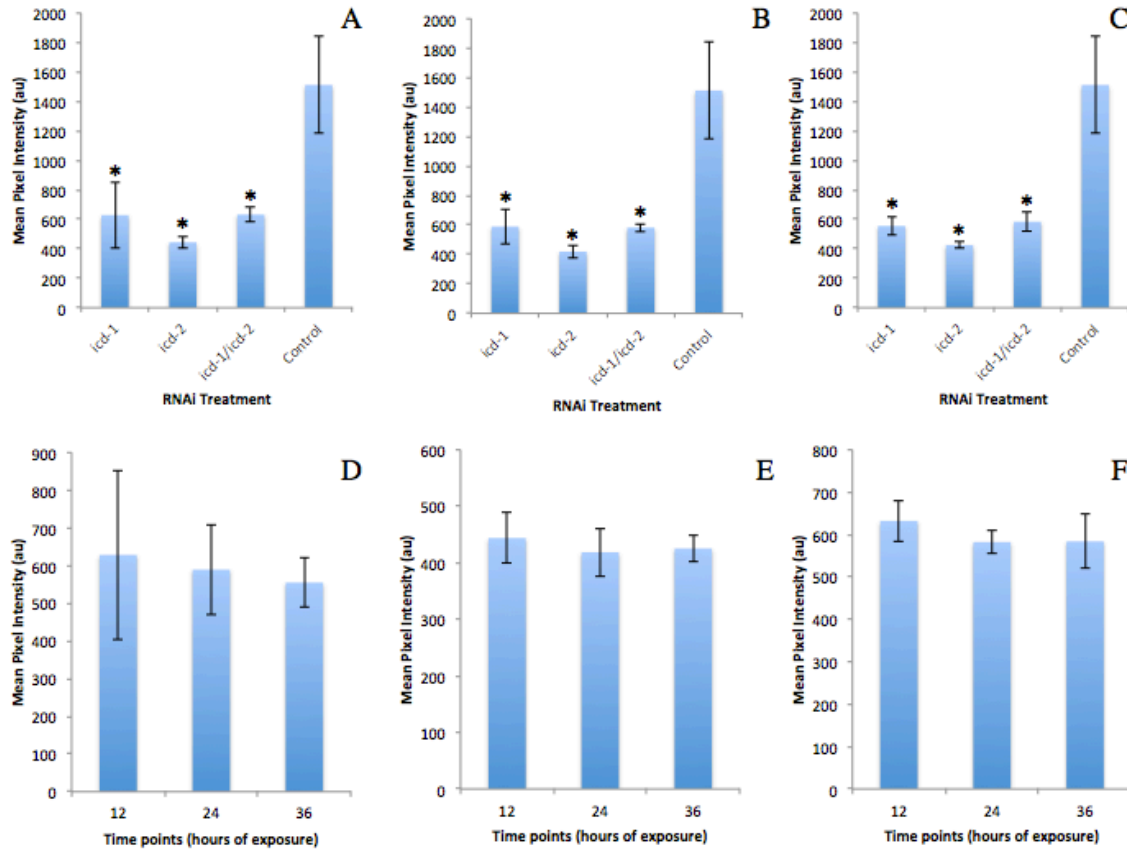


**Figure 7. Average RFP intensity levels for three-fold stage embryos exposed to specific RNAi treatments for increasing amounts of time.** *C. elegans* with a Gut::RFP expression vector were exposed to the indicated RNAi treatment or OP50-1 (*E. coli*) bacteria expressing no double stranded RNA and their progeny embryos were randomly assessed for level of RFP intensity using confocal microscopy. Images were processed to determine the mean pixel intensity with ImageJ software. (A) 12 hour time point of RNAi (*icd-1*(RNAi), *icd-2*(RNAi), or *icd-1/icd-2*(RNAi)) and control treatments. (B) 24 hour time point of RNAi (*icd-1*(RNAi), *icd-2*(RNAi), or *icd-1/icd-2*(RNAi)) and control treatments. (C) 36 hour time point of RNAi (*icd-1*(RNAi), *icd-2*(RNAi), or *icd-1/icd-2*(RNAi)) and control treatments. (D) 12, 24, and 36 hour time points for *icd-1*(RNAi) treatment. (E) 12, 24, and 36 hour time points for *icd-2*(RNAi) treatment. (F) 12, 24, and 36 hour time points for *icd-1/icd-2*(RNAi) treatment. Black asterisks indicate statistically significant difference between RNAi treatment and control treatment. Red asterisks indicate statistically significant difference between RNAi treatments. Blue asterisks indicate statistically significant difference between time points.

The mean intensity values (arbitrary units) for four-fold stage embryos exposed to *icd-1*(RNAi) treatment by time points (12 hours, 24 hours, and 36 hours) were:  $589.44 \pm 244.27$ ,  $606.03 \pm 76.55$ , and  $510.19 \pm 75.58$ , respectively while those exposed to *icd-*

2(RNAi) treatment by time points (12 hours, 24 hours, and 36 hours) were:  $436.63 \pm 53.70$ ,  $409.83 \pm 45.58$ , and  $420.30 \pm 27.45$ , respectively. The mean intensity values for four-fold embryos exposed to *icd-1/icd-2*(RNAi) treatment by time points (12 hours, 24 hours, and 36 hours) were:  $594.01 \pm 54.52$ ,  $603.34 \pm 53.50$ , and  $619.86 \pm 66.25$ , respectively. The mean intensity value for the control treatment was  $1481.96 \pm 295.83$  (Table 7).

**Table 7.** Average intensity of RFP signal in four-fold embryos after exposure to specific RNAi treatments over time. Mean pixel intensity (arbitrary units) for four-fold stage embryos exposed to *icd-1*(RNAi), *icd-2*(RNAi), or *icd-1/icd-2*(RNAi) were determined every 12 hours for 36 hours as a measure of RFP signal intensity and expressed as an average.

<b>Four-fold Mean Intensity</b>				
	<i>icd-1</i> (RNAi)	<i>icd-2</i> (RNAi)	<i>icd-1/icd-2</i> (RNAi)	<b>Control</b>
<b>12 hours</b>	$589.44 \pm 244.27$	$436.63 \pm 53.70$	$594.01 \pm 54.52$	$1481.96 \pm 295.83$
<b>24 hours</b>	$606.03 \pm 76.55$	$409.83 \pm 45.58$	$603.34 \pm 53.50$	
<b>36 hours</b>	$510.19 \pm 75.58$	$420.30 \pm 27.45$	$619.86 \pm 66.25$	

The mean pixel intensity data were analyzed with a two-way ANOVA to determine the statistical significance between the treatments for each time point (Figure 8A-C). When the 12 hour time point of the four-fold stage embryos was compared, RNAi (*icd-1*(RNAi), *icd-2*(RNAi), or *icd-1/icd-2*(RNAi)) and control treatments had statistically significant differences with a p-value of  $<0.0001$ . A Tukey post-hoc test indicated that the differences lie between the RNAi (*icd-1*(RNAi), *icd-2*(RNAi), or *icd-1/icd-2*(RNAi)) treatments and the control treatment with an alpha value of 0.05. When the 24 hour time point of the four-fold stage embryos was compared, RNAi (*icd-1*(RNAi), *icd-2*(RNAi), or *icd-1/icd-2*(RNAi)) and control treatments had statistically significant differences with a p-value of  $<0.0001$ . A Tukey post-hoc test indicated that

the differences lie between the RNAi (*icd-1*(RNAi), *icd-2*(RNAi), or *icd-1/icd-2*(RNAi)) treatments and the control treatment with an alpha value of 0.05. Additionally, the post-hoc test indicated statistically significant differences between *icd-1*(RNAi) and *icd-2*(RNAi) treatments with an alpha value of 0.05. When the 36 hour time point of the four-fold stage embryos was compared, RNAi (*icd-1*(RNAi), *icd-2*(RNAi), or *icd-1/icd-2*(RNAi)) and control treatments had statistically significant differences with a p-value of <0.0001. A Tukey post-hoc test indicated that the differences lie between the RNAi (*icd-1*(RNAi), *icd-2*(RNAi), or *icd-1/icd-2*(RNAi)) treatments and the control treatment with an alpha value of 0.05.

The mean pixel intensity unit data were also analyzed with a two-way ANOVA to determine the statistical significance between the time points within each treatment (Figure 8D-F). When the four-fold stage embryos exposed to *icd-1*(RNAi) treatment were compared, the 12 hour, 24 hour, and 36 hour did not have a statistically significant difference with a p-value of 0.2916. When the four-fold stage embryos exposed to *icd-2*(RNAi) treatment were compared, 12 hour, 24 hour, and 36 hour did not have a statistically significant difference with a p-value of 0.3640. When the four-fold stage embryos exposed to *icd-1/icd-2*(RNAi) treatment were compared, 12 hour, 24 hour, and 36 hour did not have a statistically significant difference with a p-value of 0.6906.

At the 12 hour, 24 hour, and 36 hour time point of exposure to RNAi treatments, the four-fold stage embryos exposed to *icd-2*(RNAi) treatment had the smallest value of mean pixel intensity while the control treatment had the largest value (Figure 8A-C). Under *icd-1*(RNAi) treatment, the four-fold embryos within the 24 hour time point had the largest value (Figure 8D). Under the *icd-2*(RNAi) treatment, the four-fold embryos

within the 12 hour time point had the largest value (Figure 8E). Under the *icd-1/icd-2*(RNAi) treatment, the four-fold embryos within the 36 hour time point had the largest value (Figure 8F).

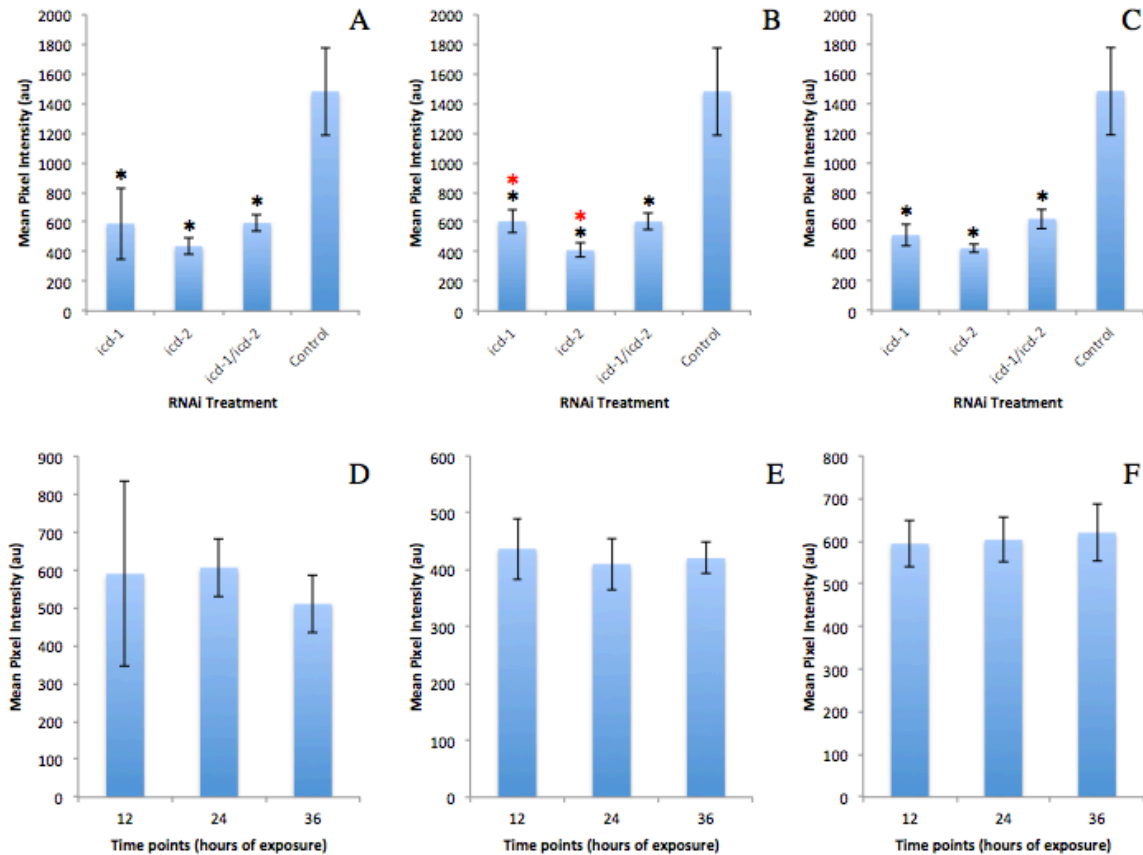


**Figure 8. Average RFP intensity levels for four-fold stage embryos exposed to specific RNAi treatments for increasing amounts of time.** *C. elegans* with a Gut::RFP expression vector were exposed to the indicated RNAi treatment or OP50-1 (*E. coli*) bacteria expressing no double stranded RNA and their progeny embryos were randomly assessed for level of RFP intensity using confocal microscopy. Images were processed to determine the mean pixel intensity with ImageJ software. (A) 12 hour time point of RNAi (*icd-1*(RNAi), *icd-2*(RNAi), or *icd-1/icd-2*(RNAi)) and control treatments. (B) 24 hour time point of RNAi (*icd-1*(RNAi), *icd-2*(RNAi), or *icd-1/icd-2*(RNAi)) and control treatments. (C) 36 hour time point of RNAi (*icd-1*(RNAi), *icd-2*(RNAi), or *icd-1/icd-2*(RNAi)) and control treatments. (D) 12, 24, and 36 hour time points for *icd-1*(RNAi) treatment. (E) 12, 24, and 36 hour time points for *icd-2*(RNAi) treatment. (F) 12, 24, and 36 hour time points for *icd-1/icd-2*(RNAi) treatment. Black asterisks indicate statistically significant difference between RNAi treatment and control treatment. Red asterisks indicate statistically significant difference between RNAi treatments. Blue asterisks indicate statistically significant difference between time points.

The mean pixel intensity data were also analyzed with a Student's T-test to determine the statistical significance between the stages for each time point within each treatment (Table 8). The comparisons of each individual time point for each specific

RNAi treatment between the two stages of embryos did not show any statistically significant differences as indicated by p-values greater than 0.05 (Table 8).

**Table 8.** Calculated p-values from Student's T-tests for the comparison of the mean pixel intensity of three-fold and four-fold stage embryos relative to each other.

	<i>icd-1</i> RNAi			<i>icd-2</i> RNAi			<i>icd-1/icd-2</i> RNAi		
	12 hours	24 hours	36 hours	12 hours	24 hours	36 hours	12 hours	24 hours	36 hours
<b>p-value</b>	0.6752	0.6217	0.1234	0.7344	0.5393	0.6353	0.1367	0.3342	0.2660

#### Colocalization of HSP-4::GFP/Gut::RFP under control treatment

Previous studies on the management of misfolded protein stress in *C. elegans* identified cell-types specific differences in stress response outcomes induced by depletion of the NAC. Neurons appeared more sensitive to apoptosis in response to misfolded protein stress relative to other cell types, e.g. gut cells, due possibly to the sub-optimal expression of the UPR-specific chaperone HSP-4<sup>16,18</sup>. These studies speculate as to, but do not confirm, the nature of the cell types expressing and not expressing detectable levels of HSP-4 in response to misfolded protein stress. To determine if gut cells are resistant to NAC-depletion induced apoptosis due to the upregulation of HSP-4, we planned to determine the putative co-localization of the HSP-4::green fluorescent protein (GFP) reporter protein with Gut::RFP. Before these experiments can be performed though, we established the localization patterns of both fluorescent proteins in untreated animals.

To establish a baseline expression pattern that will allow us to characterize the effect of NAC individual subunit depletion on the colocalization of gut cells and heat shock protein 4 (HSP-4), untreated embryos expressing both reporter constructs were allowed to develop into adults (48 hours post first cleavage) and subsequently examined for Gut::RFP and HSP-4::GFP. Adult worms were observed with confocal microscopy to

determine a baseline expression of signal for HSP-4::GFP and Gut::RFP signals. Once images were captured, fluorescent signal was quantified by calculating mean colocalized pixels per area unit (arbitrary units), which was  $0.6337 \pm 0.0734$ . The adults were analyzed with a Colocalization program within ImageJ (National Institute of Health) to give an output image with only the colocalized areas to determine the amount of overlapping signal from the HSP-4::GFP signal and the Gut::RFP signal. Additionally, all fluorescent channels and DIC images were overlaid to show colocalization patterns. Colocalization, as indicated by the yellow color, was primarily localized to the anterior and posterior regions of the gut (Figure 9).

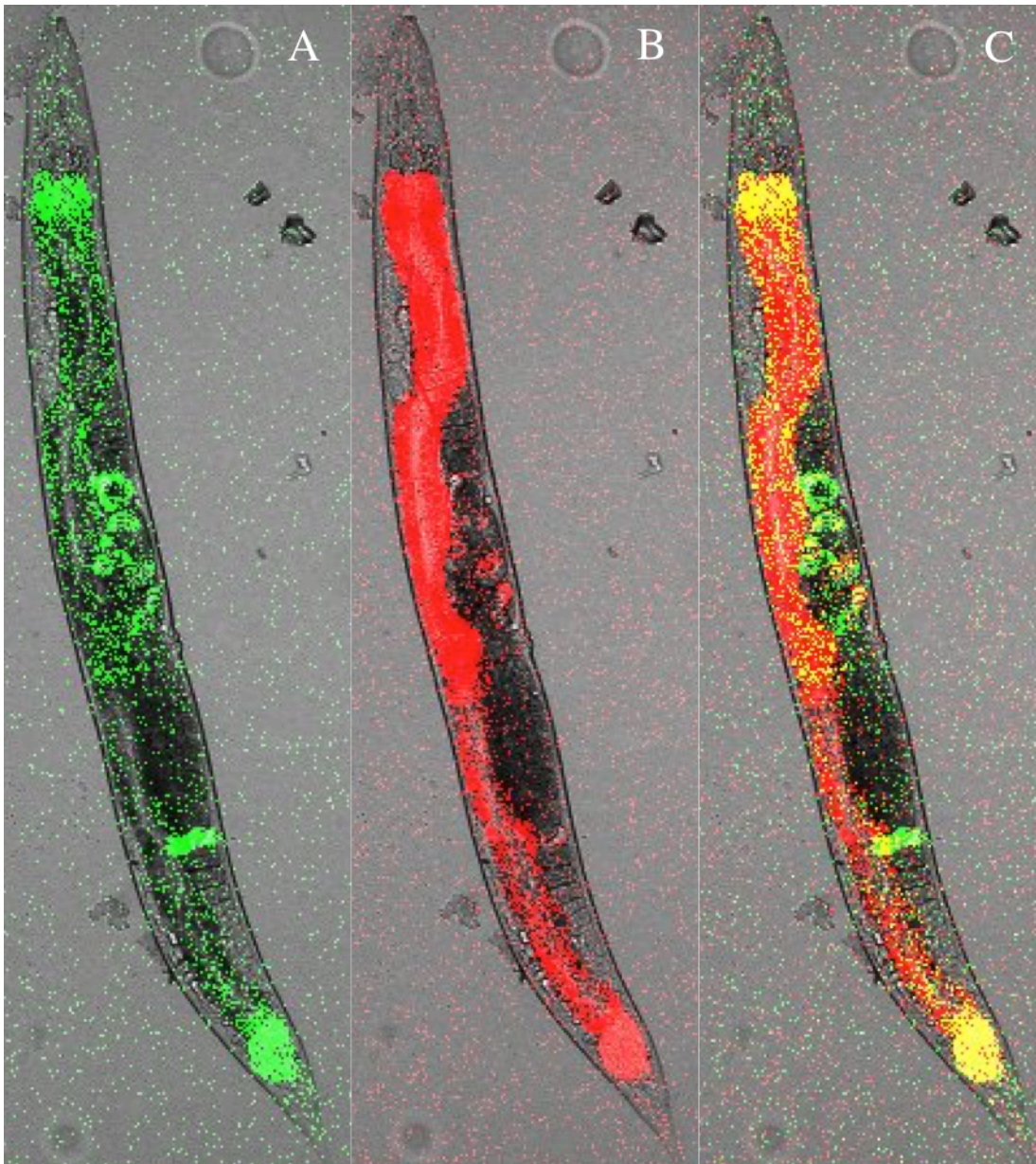


**Figure 9. Adult HSP-4::GFP/Gut::RFP worm under control treatment.** *C. elegans* with the *hsp-4::GFP* and *Gut::RFP* expression vectors were fed OP50-1 (*E. coli*) bacteria expressing no double stranded RNA and their progeny embryos were allowed to develop into adults and were randomly assessed for RFP and GFP expression with confocal microscopy. DIC and fluorescent images were overlaid with ImageJ software. (A) GFP signal overlaid with DIC image, (B) RFP signal overlaid with DIC image, (C) GFP and RFP signal overlaid with DIC image. Co-localized pixels are visualized as yellow.

## **DISCUSSION**

Historically, investigations of the function of the nascent polypeptide-associated complex (NAC) in *C. elegans* have been conducted in the context of beta subunit depletions. These studies lack the depletion of the entire complex and, instead leave the alpha subunit in relative excess. Previous research has indicated that there are individual functions that each subunit can perform when not complexed with its binding partner. Alpha NAC has been implicated as a transcription factor regulating cell differentiation<sup>22-</sup><sup>25</sup>. Conversely, beta NAC has not been as well characterized as alpha NAC as an individual subunit, but was originally identified as a transcription factor, and may play a role as a cytosolic chaperone when not bound by alpha NAC<sup>15</sup>. From previous research, one can conclude that these subunits likely function independently and therefore, phenotypes associated with the depletion of one subunit may be related to the loss of the NAC, the activity of the other subunit, or both. These studies investigated the depletion of individual subunits and the depletion of both subunits simultaneously to determine any differential effects as related to gut cell development and viability.

The level of Gut::RFP signal is indicative of the amount of this peroxisomal fusion protein present in the organism. A relatively low level of this protein could result from two outcomes: fewer peroxisomes present in the gut cells or fewer gut cells present in the organism. The first scenario could result from no significant change in the number of differentiated gut cells but rather, is a measure of the number of peroxisomes. The second scenario could result from a significant change in the number of differentiated gut cells indicated by the number of peroxisomes present within each cell. For the remainder

of this interpretation, we are hypothesizing that changes in peroxisome RFP signal are due to an effect on gut cell differentiation, and not on peroxisome biogenesis.

From the data presented, the percentage of Gut::RFP signal present within the three-fold and four-fold staged embryos showed a significant difference when comparing all RNAi treatments with the controls. Specifically, parental worms exposed to any NAC subunit depletion produced fewer embryos with Gut::RFP signal relative to untreated controls (Table 1 and 2). As such, depletion of alpha NAC, beta NAC or both affected the likelihood of progeny embryos displaying RFP signal. One interpretation of these results is a loss of gut cells in embryos unable to cope with the misfolded protein stress present, leading to debilitation and perhaps even death. Conversely, those embryos that do express Gut::RFP in the face of the misfolded protein stress may have generated a robust stress response that maintains the viability of the gut cell. This response may also display different phenotypic profiles depending specifically on the corresponding depletion. To characterize such putative differences, we proceeded to quantify the Gut::RFP signals generated in the RNAi treatment populations. When interpreting data, one must consider that this is a narrowed population view in terms of those embryos that survived the RNAi (*icd-1*(RNAi) *icd-2*(RNAi), or *icd-1/icd-2*(RNAi)) treatments and also expressed detectible Gut::RFP signal.

Mean pixels per area unit quantifies the number of pixels throughout an individual embryo. This assessment can be used as a direct measure of level of peroxisomal fusion protein expression within the embryo and, therefore, the number of peroxisomes within gut cells. Overall, the three-fold and four-fold stages of the RNAi (*icd-1*(RNAi) *icd-2*(RNAi), or *icd-1/icd-2*(RNAi)) treatments showed a significant increase in mean pixels

per area unit from the control treatment. Under the previous assumption that Gut::RFP signal is indicative of the number of gut cells, this increase in mean pixels per area unit could indicate a larger number of differentiated gut cells. Premature or atypical differentiation is a documented response to cell stress in other organisms, which could explain this increase in gut cells during NAC depletion in *C. elegans*. Notably, within the 12 hour time point, all RNAi treatments were significantly different from each other in terms of average RFP signal generated. These results support the hypothesis that phenotypes associated with depletion of one subunit may be the result of both the loss of the NAC and the activity of the remaining, unbound subunit. This difference suggests that when in excess of its binding partner, the alpha or beta subunit has different functions within the cell than they do when in complex with each other. When comparing the average RFP signal generated in each population, trends emerge: *icd-1*(RNAi) had the largest average RFP signal per embryos followed by *icd-2*(RNAi) and the *icd-1/icd-2*(RNAi). The *icd-1*(RNAi) has excess alpha NAC present relative to beta NAC and also has the highest value of mean pixels per area unit that could indicate more differentiated gut cells. These results are consistent with alpha NAC's known roles in other systems as a transcription factor associated with cell differentiation<sup>22,24,25</sup>. In those cases, alpha NAC facilitates the differentiation of cells that generate high levels of protein at some point during their progression, e.g. the making of bone matrix as an osteoblast converts to an osteocyte<sup>22,23</sup>. These results are also consistent with stress-induced differentiation of mammalian intestinal and esophageal cells undergoing misfolded protein stress<sup>26</sup>.

Mean pixel intensity quantifies the number of Gut::RFP fusion proteins occupying a defined space within the cell. This measurement could be indicative of two

different phenomena: the inappropriate differentiation of other cell types under stress to become gut cells, or the premature differentiation of stressed gut cells relative to other gut cells within the same organism. In the former situation weak Gut::*RFP* pixel intensity may be due to inappropriate differentiation of cells not destined to become gut cells. This situation could be interpreted in relation to the functionality of the peroxisomes; these cells were never intended to be gut cells, and therefore may have a decreased capacity to make peroxisomes relative to normal gut cells, resulting in decreased mean pixel intensity. The second interpretation of differential Gut::*RFP* pixel intensity would potentially indicate the premature differentiation of a gut cell. If misfolded protein stress has driven a gut cell to differentiate prematurely, the accumulation of peroxisomes would be greater in those cells relative to neighboring gut cells that may have differentiated in the appropriate time frame. Therefore, a higher mean pixel intensity could be the result of misfolded protein stress driving a gut cell to differentiate prematurely.

Future studies to distinguish between inappropriate differentiation and the specific timing of differentiation could observe individual cells destined to develop into gut cells. These cell lineage observations would follow each individual cell throughout their development during depletion of the individual subunits of the NAC to monitor the specific time and place of differentiation as determined by the appearance of the reporter signal. Individual gut cell boundaries could be marked to quantify the number of individual peroxisomes within the cell. This assessment would distinguish between an increase in number of peroxisomes in gut cells versus an increase in gut cells and therefore the number of peroxisomes. The three-fold and four-fold stages of the RNAi

(*icd-1*(RNAi) *icd-2*(RNAi), and *icd-1/icd-2*(RNAi)) treatments showed a significant decrease in mean pixel intensity from the control treatment. This suggests that there were gut cells that differentiated inappropriately due to the cell stress response and these gut cells have lower functionality within their peroxisomes than the gut cells that were destined to differentiate under normal cellular conditions. The lower functionality of the peroxisomes is indicated by the significant decrease in the reporter fusion protein that is produced within peroxisomes. Overall, *icd-1*(RNAi) had a larger mean pixel intensity value than *icd-2*(RNAi) and was statistically significant at the 24 hour time point of the four-fold stage embryos. As previously stated, RNAi assays have a spectrum of effects within the treatment, the range of data values for the majority of the reported time points for both stages of embryos does not indicate any significance. With the continuation of trials, more distinct and statistically significant trends may emerge to support the preliminary evidence that we have defined at the 24 hour time point for four-fold stage embryos.

From the conducted Student's T-test between the three-fold stage and four-fold stage embryos values for mean pixels per area unit and the mean pixel intensity, overall, no significant difference was found. The only statistically significant difference between the three-fold and four-fold stage embryos was during *icd-1*(RNAi) treatment at the 24 hour time point and as such, no discernable trend in differences can be made between the two stages of embryos. In general, all RNAi treatments in both stages of embryos rendered the same trends: more gut cells differentiated inappropriately as indicated by the higher amount of mean pixels per area unit compared to the control treatment. However, this increase in differentiated gut cells resulting from all RNAi treatments did not

generate cells with the same functionality or the same time of differentiation as the control treatment as indicated by mean pixel intensity. These results may indicate that misfolded protein stress may be driving cells into early or atypical gut cell differentiation, but these cells are not adhering to a fully completed differentiation program, resulting in partially functional gut cells.

Along with differentiation as a response to cell stress, the upregulation of chaperones can also occur, depending on cell type. Heat shock protein 4 (HSP-4) has been previously studied as a chaperone that is upregulated specifically during times of misfolded protein stress in the ER of *C. elegans*<sup>12</sup>. From these findings, there is evidence that the individual NAC subunits have functions related to the regulation of differentiation. We are now interested to determine how specific cell types respond to misfolded protein stress through upregulation of HSP-4. Increased expression of HSP-4 indicates the engagement of UPR mechanisms focused on saving the cell and avoiding the initiation of apoptosis.

The *hsp-4::GFP/Gut::RFP* reporter strain combines the ability to use HSP-4::GFP signal as a reporter for the management of cell stress with the ability to specifically identify gut cells within the animal. Using this co-expressing strain, we can now specifically monitor the expression of HSP-4, a cell saving UPR outcome, in gut cells in real time. These data establishes baseline co-localization data of HSP-4::GFP and Gut::RFP for comparison with localization data gathered from *icd-1*(RNAi), *icd-2*(RNAi), or *icd-1/icd-2*(RNAi) treatments. Future studies will investigate the RNAi (*icd-1*(RNAi) *icd-2*(RNAi), or *icd-1/icd-2*(RNAi)) treatments to determine any statistically significant deviation from this baseline control data. Additionally, future studies to

investigate other cell lineages, specifically neuronal and muscle cell lineages, would compare the cell-specific ability to manage stress in a similar way. Utilizing HSP-4::GFP as an indicator of stress management, the co-localization of cell lineage signals (gut, neuronal, and muscle) and the HSP-4::GFP would allow for the determination of cell specific stress responses. The working hypothesis is that neurons are unable to upregulate HSP-4 efficiently to cope with stress conditions resulting in a greater susceptibility to apoptosis. An accompanying hypothesis is that there are cell types such as gut and muscle cells, are able to upregulate HSP-4 effectively and resist apoptosis in the face of misfolded protein stress. This research has implications for neurodegenerative diseases in the context that neuronal cells are more susceptible to cell stress and will induce cell-killing mechanisms.

In conclusion, the protocol we've developed throughout this research has optimized the parameters used to determine the effects of NAC depletion on cell differentiation, specifically in the gut cells of *C. elegans*. With this methodology, differentiation of muscle and neuronal cells in NAC-depleted *C. elegans* can be observed and quantified using confocal microscopy to determine cell-type specific differentiation patterns under stress conditions. Furthermore, our work provides a framework for determining the upregulation of HSP-4 as a cell specific stress responses for gut, muscle, and neuronal cells in NAC-depleted *C. elegans*. These future studies will elucidate any differences in cell-type specific responses to misfolded protein stress, providing insights into why certain cell types are more susceptible to death during misfolded protein stress, and how this sensitivity could contribute to the development of disease.

## **ACKNOWLEDGMENTS**

We would like to collectively thank Dr. Tim Bloss for everything he has done for us over the past three years. Additionally, we would like to thank our committee members, Dr. Kim Slekar and Dr. Kyle Seifert. Also, thank you to the Bloss laboratory members and Christophe Langouet for his help with statistical analysis.

## REFERENCES

1. Baldwin. Energetics of Protein Folding Kinetics. *Biophys. J.* **102**, 58a (2012).
2. Ciryam, P., Tartaglia, G., Morimoto, R. I., Dobson, C. M. & Vendruscolo, M. Widespread Aggregation and Neurodegenerative Diseases Are Associated with Supersaturated Proteins. *Cell Rep.* **5**, 781–790 (2013).
3. Gardner, B. M., Pincus, D., Gotthardt, K., Gallagher, C. M. & Walter, P. Endoplasmic reticulum stress sensing in the unfolded protein response. *Cold Spring Harb Perspect Biol* **5**, a013169 (2013).
4. Malhotra, J. D. & Kaufman, R. J. The endoplasmic reticulum and the unfolded protein response. *Semin. Cell Dev. Biol.* **18**, 716–731 (2007).
5. Hetz, C. The unfolded protein response: controlling cell fate decisions under ER stress and beyond. *Nat. Rev. Mol. Cell Biol.* (2012). doi:10.1038/nrm3270
6. Voisine, C., Pedersen, J. S. & Morimoto, R. I. Chaperone networks: Tipping the balance in protein folding diseases. *Neurobiol. Dis.* **40**, 12–20 (2010).
7. Liu, Y. & Chang, A. Heat shock response relieves ER stress. *EMBO J.* **27**, 1049–1059 (2008).
8. Brehme, M. *et al.* A Chaperome Subnetwork Safeguards Proteostasis in Aging and Neurodegenerative Disease. *Cell Rep.* **9**, 1135–1150 (2014).
9. Schmidt, M. & Finley, D. Regulation of proteasome activity in health and disease. *Biochim. Biophys. Acta* **1843**, 13–25 (2014).
10. Hartl, F. U. & Hayer-Hartl, M. Molecular chaperones in the cytosol: from nascent chain to folded protein. *Science* **295**, 1852–1858 (2002).
11. Hartl, F. U., Bracher, A. & Hayer-Hartl, M. Molecular chaperones in protein folding and proteostasis. *Nature* **475**, 324–332 (2011).
12. Bozaykut, P., Ozer, N. K. & Karademir, B. Free Radical Biology and Medicine Regulation of protein turnover by heat shock proteins. *Free Radic. Biol. Med.* **77**, 195–209 (2014).
13. Lu, R. *et al.* Heat Shock Protein 70 in Alzheimer ' s Disease. **2014**, (2014).
14. Doyle, S. M., Genest, O. & Wickner, S. Protein rescue from aggregates by powerful molecular chaperone machines. *Nat. Rev. Mol. Cell Biol.* **14**, 617–29 (2013).

15. Beatrix, B., Sakai, H. & Wiedmann, M. The  $\alpha$  and  $\beta$  subunit of the nascent polypeptide-associated complex have distinct functions. *J. Biol. Chem.* **275**, 37838–37845 (2000).
16. Arsenovic, P. T., Maldonado, A. T., Colletuori, V. D. & Bloss, T. a. Depletion of the C. elegans NAC Engages the Unfolded Protein Response, Resulting in Increased Chaperone Expression and Apoptosis. *PLoS One* **7**, (2012).
17. Kirstein-Miles, J., Scior, A., Deuerling, E. & Morimoto, R. I. The nascent polypeptide-associated complex is a key regulator of proteostasis. *EMBO J.* **32**, 1451–68 (2013).
18. Bloss, T. a, Witze, E. S. & Rothman, J. H. Suppression of CED-3-independent apoptosis by mitochondrial betaNAC in Caenorhabditis elegans. *Nature* **424**, 1066–1071 (2003).
19. Guo, B. *et al.* The nascent polypeptide-associated complex is essential for autophagic flux. *Autophagy* **10**, 37–41 (2014).
20. Rutkowski, D. T. & Hegde, R. S. Regulation of basal cellular physiology by the homeostatic unfolded protein response. *J. Cell Biol.* **189**, 783–794 (2010).
21. Hetz, C. & Glimcher, L. H. Fine-Tuning of the Unfolded Protein Response: Assembling the IRE1 $\alpha$  Interactome. *Mol. Cell* **35**, 551–561 (2009).
22. Yotov, W. V, Moreau, a & St-Arnaud, R. The alpha chain of the nascent polypeptide-associated complex functions as a transcriptional coactivator. *Mol. Cell. Biol.* **18**, 1303–1311 (1998).
23. Moreau, a, Yotov, W. V, Glorieux, F. H. & St-Arnaud, R. Bone-specific expression of the alpha chain of the nascent polypeptide-associated complex, a coactivator potentiating c-Jun-mediated transcription. *Mol. Cell. Biol.* **18**, 1312–1321 (1998).
24. Jafarov, T., Alexander, J. W. M. & St-Arnaud, R.  $\alpha$ NAC interacts with histone deacetylase corepressors to control Myogenin and Osteocalcin gene expression. *Biochim. Biophys. Acta - Gene Regul. Mech.* **1819**, 1208–1216 (2012).
25. Meury, T., Akhouayri, O., Jafarov, T., Mandic, V. & St-Arnaud, R. Nuclear alpha NAC influences bone matrix mineralization and osteoblast maturation in vivo. *Mol. Cell. Biol.* **30**, 43–53 (2010).
26. Lopez, S. *et al.* NACA is a positive regulator of human erythroid-cell differentiation. *J. Cell Sci.* **118**, 1595–1605 (2005).

27. Thiede, B., Dimmler, C., Siejak, F. & Rudel, T. Predominant Identification of RNA-binding Proteins in Fas-induced Apoptosis by Proteome Analysis. *J. Biol. Chem.* **276**, 26044–26050 (2001).
28. Brockstedt, E., Otto, A., Rickers, A., Bommert, K. & Wittmann-Liebold, B. Preparative high-resolution two-dimensional electrophoresis enables the identification of RNA polymerase B transcription factor 3 as an apoptosis-associated protein in the human BL60-2 Burkitt lymphoma cell line. *J. Protein Chem.* **18**, 225–231 (1999).
29. Kogan, G. L. & Gvozdev, V. a. Multifunctional nascent polypeptide-associated complex (NAC). *Mol. Biol.* **48**, 189–196 (2014).